Natural Resources Canada | Ressources naturelles Canada

GEOLOGICAL SURVEY OF CANADA
OPEN FILE 7995

SASKATCHEWAN GEOLOGICAL SURVEY
MISCELLANEOUS REPORT 2016-3

Porosity and permeability evaluation for the Devonian-Mississippian Lower Middle Bakken Member in the Viewfield Pool, southeastern Saskatchewan

K. Hu, D. Kohlruss, C. Yang, and Z. Chen

2017

GEOLOGICAL SURVEY OF CANADA
OPEN FILE 7995
SASKATCHEWAN GEOLOGICAL SURVEY
MISCELLANEOUS REPORT 2016-3

Porosity and permeability evaluation for the Devonian-Mississippian Lower Middle Bakken Member in the Viewfield Pool, southeastern Saskatchewan

K. Hu[1], D. Kohlruss[2], C. Yang[2], and Z. Chen[1]

[1] Geological Survey of Canada, 3303-33rd Street NW, Calgary, Alberta
[2] Saskatchewan Geological Survey, Saskatchewan Ministry of the Economy, Regina, Saskatchewan

2017

doi:10.4095/300079

This publication is available for free download through GEOSCAN (http://geoscan.nrcan.gc.ca/).

Recommended citation
Hu, K., Kohlruss, D., Yang, C., and Chen, Z., 2017. Porosity and permeability evaluation for the Devonian-Mississippian Lower Middle Bakken Member in the Viewfield Pool, southeastern Saskatchewan; Geological Survey of Canada, Open File 7995, 47 p. (*also* Saskatchewan Geological Survey, Miscellaneous Report 2016-3). doi: 10.4095/300079

Publications in this series have not been edited; they are released as submitted by the author.

CONTENTS

SUMMARY

The Bakken Formation in southeastern Saskatchewan comprises three distinct members. The Upper and Lower members are black, organic-rich shales and are widely recognized as world-class source rocks for oil and gas. The Middle Bakken siltstones and sandstones have been the focus of massive horizontal drilling programs in recent years with highly variable success. The Middle Bakken Member has been divided into three distinct units: A, B, and C (Kohlruss and Nickel, 2009, 2013). Over 2700 horizontal production wells with hydraulic fracturing have been drilled in the Viewfield Pool, which is located between Townships 6 to11, Ranges 6W2 to 11W2 in southeastern Saskatchewan. The main drilling target is Unit A, the lowest unit of the Middle Bakken Member. The Viewfield Bakken play has been described as an unconventional play due to its extreme low permeability (Kohlruss and Nickel, 2012). Reservoir evaluation, such as accurate determination of porosity and permeability, has always been challenging because of low permeability, the complexity of lithology and reservoir heterogeneity.

This study focuses on reservoir characterization of Unit A of the Middle Bakken Member in the Viewfield Pool. By a thorough analysis of core measurements, conventional well logs and available advanced nuclear magnetic resonance (NMR) well log data, we have completed a core-log integration and developed petrophysical models for estimating reservoir porosity and permeability using conventional well logs. Subsequently, the effectiveness of the method will be evaluated in the Bakken Viewfield oil pool.

Proposed porosity models include a well log-based bulk volume model and a core-based model. With matrix parameter and clay corrections, the volume model has been used to establish five equations to calculate reservoir porosity using single-log sonic, density, neutron, and dual-log combination of density-sonic and neutron-density logs. The core-based method is based on integration of core and log data, including core-sonic and core-density models for porosity calculation.

Comparing log-derived porosity with measured core porosity for Unit A, porosity calculated from the density volume equation gives the best match and the neutron-density volume method provides good porosity calculation results. The core-density model also results in an accurate porosity calculation and the density-sonic volume method provides a fair porosity calculation

result. Most porosity values from single sonic and neutron models are reasonable estimates, even though sometimes the results are slightly higher than core measurements.

A combined core-based permeability and core-NMR permeability model for Unit A is proposed, resulting in a reasonable permeability estimation that is comparable to core measurements. Furthermore, a proposed density volume porosity model and a core-NMR permeability model have been applied for Unit A of the Middle Bakken Member in the Viewfield area, presenting reservoir quality distributions and correlations of porosity and permeability along six cross sections.

INTRODUCTION

The Upper Devonian-Lower Mississippian Bakken Formation has fast become one of the hottest onshore oil plays of this decade, revitalizing considerable interest throughout the Williston Basin. The Bakken Formation comprises three members. The Upper and Lower members are black organic-rich shales and the Middle Bakken siltstones and sandstones are sandwiched in between. Kohlruss and Nickel (2009, 2013) divided the Middle Bakken Member into three distinct units: A, B, and C, using the parameters set from core and well logs (Figure 1).

The Viewfield Pool is located between Townships 6 to 11, Ranges 6W2 to 11W2 in southeastern Saskatchewan (Figure 2). Over 2700 horizontal production wells with hydraulic fracturing have been drilled in the Viewfield Pool since 2005 (Kohlruss and Nickel, 2013; Kohlruss et al., 2013; Cronkwright et al., 2014). The main drilling target is Unit A, the lowest unit of the Middle Bakken Member, which primarily consists of dolomitic fine-grained sandstone, dolomitic siltstone, and calcareous siltstone, with a small amount of silty wackestone (Christopher, 1961; Kohlruss and Nickel, 2009; Angulo and Buatois, 2011; Staruiala et al., 2013). The porosity and permeability are closely related to and/or controlled by lithofacies (Zhao and Qing, 2014). The Viewfield Bakken play has been described as an unconventional play due to its extreme low permeability (Kohlruss and Nickel, 2012). The low formation permeability, coupled with the complex lithology and depositional history has caused challenges for evaluation of reservoir properties, especially accurate determination of its porosity and permeability.

The objective of this study is to conduct petrophysical analysis and reservoir characterization for the Middle Bakken Member in the Viewfield Pool, including 1) to analyze

core data from 45 wells and NMR logs acquired from three wells in the study area; 2) to develop petrophysical models for calculating reservoir porosity and permeability for Unit A by approaches that integrate laboratory core measurements with NMR porosity, permeability and conventional well logs; and 3) to reveal reservoir heterogeneity across the study area through well-to-well correlations along six cross sections of Unit A in the Viewfield area. Part of the study results were published in a Canadian Society of Petroleum Geologists poster (Hu et al., 2015).

LOG SIGNATURES OF THE MIDDLE BAKKEN FORMATION

The Middle Bakken Member of southeast Saskatchewan has been divided into three distinct units: A, B and C, based on lithology and petrophysical properties. Knowledge of the distribution and relationship of these units has become critical to the development of the Bakken oil resource (Kohlruss and Nickel, 2009, 2013).

Unit A unconformably overlies the Lower Bakken shale (Christopher, 1961). In the Viewfield Pool, this unit mainly consists of dolomitic fine-grained sandstone, dolomitic siltstone, and calcareous siltstone, with minor amounts of authigenic pyrite (Kohlruss and Nickel, 2009, 2013; Cronkwright et al., 2014). The unit has a maximum thickness of 11 m near the southern boundary of the pool and thins toward the northeastern pool boundary to less than 3 m (Cronkwright et al., 2014). It is the primary reservoir and producing unit in the Viewfield area. Light oil is likely to be produced from the very fine-grained sandstone in the uppermost interval of Unit A (Kreis et al., 2006).

Unit B sharply overlies Unit A and gradationally underlies Unit C. It is a fine-grained, calcite-cemented sandstone that ranges from massively bedded at the base, to high-angle planar cross-bedded, to laminated at the top (Kohlruss and Nickel, 2012).

Unit C is the uppermost portion of the Middle Bakken Member and is recognized by laminated argillaceous dolomitic siltstone to very fine-grained sandstone (Kohlruss and Nickel, 2012). Its thickness increases from 1.5 m near the southern pool boundary to more than 4 m near the northern pool boundary. Porosities are much lower in this unit compared to Unit A (Cronkwright et al., 2014).

The Middle Bakken Member is recognizable in wireline logs because of the strong contrast in lithology with the Lower and Upper members (Figure 1). A composite plot from the Viewfield Bakken play, consisting of various geophysical logs plus basic lithology interpretation, is used to illustrate typical well-log signatures for all members of the Bakken Formation (Figure 3). The combined logs on Figure 3 include the following:

- Track 1 shows the gamma ray (GR), or spectral gamma ray (SGR, if available), spontaneous potential (SP), and borehole compensated sonic transit time (DT);
- Track 2 shows the bulk density (RHOB), density porosity (PHIDls – with limestone calibration), and neutron porosity (PHINls – with limestone calibration); and
- Track 3 displays available resistivity curves, including deep (RD), medium (RM) and shallow (RS, if available) resistivity logs.

As shown in Figure 3, the upper and lower shales are characterized by an abnormally high gamma ray (>200 API) and unusually high resistivity readings, which are due to the presence of organic matter. The two organic-rich source rocks also show high sonic transit time, high neutron porosity and lower bulk density readings. In contrast, the Middle Member has a signature of clastic and carbonate rocks (Figure 3). Unit C mainly consists of dolomitic siltstone to very fine-grained sandstone, which is characterized by relatively higher gamma ray readings compared to Unit A and Unit B, fair resistivity, but high bulk density and fair sonic transit time readings due to dolomite content. For the calcite sandstone Unit B, well logs exhibit very low gamma ray readings, but higher density porosity and higher resistivity readings, illustrating a better reservoir quality than Unit C (Figure 3). Unit A is predominantly composed of grey calcareous siltstone and dolomitic siltstone, but coarsens upward into silty fine-grained sandstone in the upper part of the unit. Where thickest, Unit A is characterized by a decrease of gamma ray and bulk density readings, and an increase in sonic transit time and porosity upward from base to top. The resistivity values are generally low for the entire unit (Figure 3).

CORE ANALYSIS MEASUREMENTS

A total of 1026 core samples from 45 cored wells in the Viewfield area were examined for their rock properties, including porosity, permeability and grain density measurements that were determined in the laboratory. These core analysis data are from units A, B and C of the Middle

Bakken Member. Among them, more than 81% are from Unit A. Figures 4, 5 and 6 present histogram plots for all samples from units A, B, and C for core porosity, maximum permeability, and horizontal and vertical permeability, respectively.

In Figure 4, histogram plots of porosity are shown for units A, B and C. For Unit A, over 75% of the 836 core samples have porosity values ranging from 6% to 15%; their average is 10.4% and their median value is 11% (Figure 4a). Most (over 82% of the core samples) of the porosity values from Unit B are greater than 9% with an average of 11.1% and a median value of 11.8% (Figure 4b). The core porosity values from Unit C are distributed over a wide range, from <3% to >18%, but 66% of porosity values are mainly between 3% and 9%, with an average of 8.6% and a median value of 8.3% (Figure 4c). Unit B has the highest porosity (Figure 4b) and Unit C exhibits the lowest porosity (Figure 4c).

Figure 5 shows the distribution of core maximum permeability for the three units. The maximum permeability values for most samples of Unit A (95%) are between 0.01 and 1 mD with an average of 0.32 mD and a median of 0.13 mD (Figure 5a). About 72% of the core samples from Unit B have higher maximum permeability ranges from 0.1 to 10 mD (Figure 5b); their average value is 4.55 mD, with 0.45 mD as median. For Unit C, about 87% of samples' maximum permeability values are between 0.01 and 1 mD with an average of 1.87 mD and a median of 0.22 mD (Figure 5c). Evidently, Unit A has the lowest permeability.

Figure 6 compares the distribution of core horizontal and vertical permeability for the three units. It is evident that the horizontal permeability for all three units is higher than their vertical permeability (Figure 6). The horizontal permeability is highest for Unit B (Figure 6b).

In Figures 5 and 6, the minimum permeability value of 0.01 mD may represent the lower limit of measurement rather than the true minimum permeability value for the core samples.

For the three units, measured core grain density values are generally higher than pure quartz sandstone or siltstone (2650 kg/m^3), due to the presence of dolomite and/or calcite cements, and pyrite based on core descriptions (Kohlruss and Nickel, 2009; Cronkwright et al., 2014). For all core samples from Unit A, their average grain density is 2714 kg/m^3, with a median of 2720 kg/m^3 (Figure 7a). For Unit B, the average value of core grain density is 2702 kg/m^3, with a median of 2720 kg/m^3 (Figure 7b). Most grain density values in Unit C predominantly range from 2710 to 2770 kg/m^3 (Figure 7c), with the average and median being 2730 kg/m^3 and 2733 kg/m^3, respectively.

METHODOLOGY OF RESERVOIR EVALUATION

In general, the determination of lithology and porosity go together since both these parameters are closely linked and any error in the choice of rock type in a petrophysical model results in an erroneous porosity which can be significant. In this section, taking into consideration reservoir lithology, we mainly focus on the integration of core analysis with well log data to determine reservoir porosity and permeability for Unit A of the Middle Bakken Member in the Viewfield Pool. Insufficient core and NMR logging data is available for units B and C and only the density log is used to calculate porosity for units B and C.

Porosity determination

Two types of porosity models will be discussed, including a log-based bulk volume model and a core-based model. These porosity models are applied to Unit A of the Middle Bakken Member for estimating reservoir porosity.

Type 1: Log-based bulk volume model

Conventional density, sonic and neutron logs are widely used to determine reservoir porosity. We employ these three porosity logs for our log-based bulk volume models, which include three single-log porosity models (sonic, density and neutron), and two dual-log porosity models (density-sonic and neutron-density). For each of the bulk volume models, we assume that the log readings are affected primarily by rock matrix (i.e. composition of grains), volume of pore fluids and clay materials (if clay exists).

For a clay-free formation consisting of grains/matrix, with an average grain/matrix log value (X_{ma}), and a porosity (ϕ, fractional), filled by a fluid with an average fluid log value (X_f), the formation porosity log reading (X_{log}) will be:

$$X_{log} = \phi X_f + (1 - \phi) X_{ma} \quad (1)$$

For a shaly formation, the log response has contributions from the matrix, clay and fluids in the pores.

$$X_{log} = \phi X_f + V_{cl} X_{cl} + (1 - \phi - V_{cl}) X_{ma} \quad (2)$$

where, X_{log} is the log response of a specific log type used for determining porosity in Eq. (2) (it can be any one of the porosity logs, such as sonic, density or neutron). V_{cl} is clay content (fractional), X_{cl} is the log reading from a pure shale interval. Average grain/matrix log value (X_{ma}) depends on formation lithology, such as rock mineral or matrix components. The average fluid log value (X_f) mainly depends on formation water salinity.

Clay content

Reservoir porosity and permeability estimates are greatly affected by clay in the Middle Bakken Member of the Viewfield Pool. Clay within a reservoir must be identified and quantified so that its effects on both well logs and core measurements can be adequately understood.

The volume of clay is also an indicator of reservoir quality and can be estimated from well logs by many techniques. Two common logs used to indicate clay content are gamma ray (GR) or spectral gamma ray (SGR), and spontaneous potential (SP) logs. For this study, clay content (V_{cl}) is determined by using the GR (SGR) log for most of the wells in the Viewfield Pool:

$$V_{cl} = (GR_{log} - GR_{sd}) / (GR_{sh} - GR_{sd}) \quad (3)$$

or the spontaneous potential log (SP) is used for the wells where the GR log is not complete or questionable, or if the formation contains other radioactive components other than clay, such as K-feldspar or mica.

$$V_{cl} = (SP_{log} - SP_{sd}) / (SP_{sh} - SP_{sd}) \quad (4)$$

where V_{cl} is clay content (fractional), GR_{log} is (spectral) gamma ray log reading and SP_{log} is spontaneous potential log reading for the target layer. GR_{sh} and GR_{sd} are (spectral) gamma ray readings against pure shale layer and clay-free sand, respectively. SP_{sh} and SP_{sd} are spontaneous potential log readings for a pure shale layer and a clay-free sand, respectively.

Single-log density porosity model

Based on the bulk volume model (1), the formation bulk density (ρ_b) for a clay-free formation will be (Schlumberger, 1989):

$$\rho_b = \phi\, \rho_f + (1 - \phi)\, \rho_{ma} \quad (5a)$$

where ρ_{ma} is the average grain/matrix density, ρ_f is the average fluid density and ϕ is the formation porosity, expressed as a fraction.

or

$$\phi_D = (\rho_b - \rho_{ma}) / (\rho_f - \rho_{ma}) \quad (5b)$$

where ϕ_D is the computed density porosity.

According to equation (2), the total bulk density log reading for a shaly formation will be:

$$\rho_b = \phi\, \rho_f + V_{cl}\, \rho_{cl} + (1 - \phi - V_{cl})\, \rho_{ma} \quad (6a)$$

or

$$\phi_{DC} = \phi_D - V_{cl}\, (\rho_{cl} - \rho_{ma}) / (\rho_f - \rho_{ma}) \quad (6b)$$

where ρ_{cl} is the clay density, ϕ_{DC} is the clay corrected density porosity for a shaly formation.

If a pure shale zone is absent or the clay parameter is difficult to determine, a simplified equation is used for a density porosity calculation:

$$PHID1 = \phi_{DC} = \phi_D\, (1 - V_{cl}) \quad (7)$$

As described above, the measured core grain density values for the three units of the Middle Bakken Member are obtained from core analyses (Figure 7): with an average of 2714 kg/m^3 and a median value of 2720 kg/m^3 for Unit A; an average of 2702 kg/m^3 and a median value of 2720 kg/m^3 for Unit B; an average of 2730 kg/m^3 and a median value of 2733 kg/m^3 for Unit C, indicating the matrix is not a typical pure sandstone (2650 kg/m^3), limestone (2710 kg/m^3) or dolomite (2870 kg/m^3).

For a water saturated formation, the fluid density (ρ_f) ranges from 1000 kg/m^3 (fresh water) to 1100 kg/m^3 (salt water), which is dependent only on the formation water salinity in the study area. For a hydrocarbon bearing formation, the fluid is a mixture of hydrocarbon and formation water, resulting in a density lower than water due to the lower density of the hydrocarbons. The density can be estimated from water analysis and hydrocarbon analysis in a well test.

Knowing the grain density and fluid density, a clay-free density porosity (ϕ_D) can be calculated for units A, B and C using equation (5b). Having determined the clay content from equation (3) or (4), as well as clay density (ρ_{cl}, if available), the clay-corrected density porosity for units A, B and C of the Middle Bakken Member in the Viewfield Pool can then be determined using equation (6b) or (7).

Single-log sonic porosity model

Similarly, for clay-free consolidated formations, Wyllie (Wyllie et al., 1956) proposed a linear time-average or weighted–average relationship between porosity and transit time:

$$\Delta t = \phi\, \Delta t_f + (1 - \phi)\, \Delta t_{ma} \quad (8a)$$

or

$$\phi_S = (\Delta t - \Delta t_{ma}) / (\Delta t_f - \Delta t_{ma}) \quad (8b)$$

where Δt is the reading on a sonic log in μs/m (or μs/ft); Δt_f is the transit time of the saturating fluid; and Δt_{ma} is the transit time of matrix material. ϕ_S is computed sonic porosity.

For a shaly formation, the total sonic log reading is a combination of the matrix, clay and fluids in the pores.

$$\Delta t = \phi \Delta t_f + V_{cl} \Delta t_{cl} + (1 - \phi - V_{cl}) \Delta t_{ma} \quad (9a)$$

or

$$\phi_{SC} = \phi_S - V_{cl} (\Delta t_{cl} - \Delta t_{ma}) / (\Delta t_f - \Delta t_{ma}) \quad (9b)$$

where V_{cl} is clay content (fractional), Δt_{cl} is the clay sonic reading, and ϕ_{SC} is the clay corrected sonic porosity for a shaly formation.

If a pure shale zone is absent or a clay parameter is difficult to determine, equation (9b) is simplified, and is used for the sonic porosity calculation.

$$\text{PHIS1} = \phi_{SC} = \phi_S (1 - V_{cl}) \quad (10)$$

According to core descriptions, the mixed matrix may contain sandstone with dolomite and calcite (especially the lower portions of Unit A) and minor pyrite. However, core and thin section studies suggest that the contribution of grain density is predominantly from sandstone (siltstone) and dolostone in Unit A (Christopher, 1961; Kohlruss and Nickel, 2009; Angulo and Buatois, 2011; Staruiala et al., 2013), assuming that small amounts of calcite and pyrite have little impact on the overall grain density. The matrix is estimated to consist of 71% sandstone and 29% dolostone using an average core grain density of 2714 kg/m^3, or 67% of sandstone and 33% of dolostone if the median value of 2720 kg/m^3 is used. These percentage values of matrix components are applied to a sonic matrix parameter (Δt_{ma}) estimation of approximately 175~173 μs/m for Unit A.

Fluid sonic transit time (Δt_f) ranges from 616 μs/m (salt water) to 656 μs/m (fresh water), which mainly depends on the water salinity for the studied formation. Once the values of the mixed matrix and the mixed fluids are determined for Unit A, a clay-free sonic porosity (ϕ_S) can be calculated using equation (8b). Using the calculated clay content (V_{cl}), and the clay value

(Δt_{cl}, if available), a clay-corrected sonic porosity can be determined using equations (9b) or (10) for Unit A.

However, core description indicates that most of the 91 sandstone core samples from Unit B consist of not only sandstone and calcite, but also dolomite and pyrite, which is supported by core grain density data (Figure 7b). This illustrates that about 54% of the core samples have higher grain density than 2710 kg/m^3, mainly due to the presence of dolomite and/or pyrite. In this situation, it is hard to estimate the proportions of the four matrix components: sandstone, calcite, dolomite, and pyrite. Thus, the sonic matrix value (Δt_{ma}) cannot be estimated for Unit B.

For Unit C, both core descriptions and grain density data suggest that variable amounts of pyrite exist in the dolomitic siltstone, which may significantly affect porosity. The matrix of Unit C contains three main components: sandstone, dolomite, and pyrite, but their content percentages cannot be estimated. Therefore, the sonic matrix value (Δt_{ma}) for Unit C cannot be estimated.

Single-log neutron porosity model

The neutron porosity log is significantly affected by clay minerals. The variable amounts of clay in units A, B and C cause changes to the neutron log readings. Therefore, a clay correction must be applied to the neutron porosity calculation:

$$\phi_{NC1} = \phi_N - V_{cl}\,\phi_{Ncl} \qquad (11)$$

where ϕ_{NC1} is the clay-corrected neutron porosity, ϕ_N is the original neutron porosity and ϕ_{Ncl} is the clay neutron porosity. These may be calibrated with sandstone, limestone, or dolomite. If a pure shale zone is absent or a clay value cannot be determined, equation (11) is then simplified:

$$\phi_{NC1} = \phi_N\,(1 - V_{cl}) \qquad (12)$$

A matrix (or lithology) correction is also required in neutron porosity calculations because the mixed matrix value determined through core measurements does not match the actual lithology (rock mineralogy) of units A, B and C, regardless of the calibration scale of the neutron log used.

Since Unit A is comprised of approximately 29-33% dolomite, the apparent neutron porosity (sandstone-calibrated or limestone-calibrated) is too high. A maximum and a minimum matrix (lithology) correction value (ϕ_{NMCmax} and ϕ_{NMCmin}) are therefore calculated:

$$\phi_{NMCmax} = -0.12*0.33 = -0.0396 \qquad (13a)$$

$$\phi_{NMCmin} = -0.12*0.29 = -0.0348 \qquad (13b)$$

The neutron porosity with both a clay and matrix correction is derived as follows:

$$PHIN = \phi_{NC} = \phi_{NC1} + NCm \quad (14)$$

$PHIN/\phi_{NC}$ is a clay and matrix corrected neutron porosity. NCm is the neutron matrix correction amount, which ranges from -0.035 to -0.04 for the apparent neutron porosity log. Equation (14) is only applied to Unit A due to the uncertainty of the matrix component percentages of units B and C.

Dual-log density-sonic and neutron-density porosity models

Dual porosity log combination models are based on two of the three porosity logs (sonic, density and neutron), including density-sonic log, and neutron-density log combinations, which are listed below:

$$PHDS = \phi_{DS} = (\phi_{DC} + \phi_{SC})/2 \quad (15)$$

$$PHND = \phi_{ND} = (\phi_{NC} + \phi_{DC})/2 \quad (16)$$

where $PHDS/\phi_{DS}$ is the density-sonic porosity; $PHND/\phi_{ND}$ is the neutron-density porosity. ϕ_{DC}, ϕ_{SC} and ϕ_{NC} are the clay-matrix corrected density, sonic and neutron porosities from the volume model, respectively.

Computed porosities from the volume models for Unit A

All the volume porosity models discussed above can be used to calculate porosity for Unit A. In the following discussion, the proposed volume porosity models are applied to Unit A in cored wells and the calculation results are presented.

Among the 45 cored wells containing the Middle Bakken Member, 38 sonic, 26 density and 25 neutron well logs were run. Figure 8 shows comparisons of measured core porosity with the calculated porosities from single porosity logs using equations (7), (10), (12) and (14). Figure 9 illustrates comparisons of measured core porosity with calculated porosities from the dual porosity log combination method using equations (15) and (16). In a comparison of the core porosity measurement, the computed porosity values derived from the proposed density porosity log incorporating the matrix and clay corrections of equation (7) provides a good match (Figure 8a), and the computed sonic porosities with matrix and clay corrections using equation (10) yields fair to good matches even though they result in slightly higher estimates for some intervals (Figure 8b). Most of the clay-corrected neutron porosity values using equation (12) are consistently higher than core measurements before a matrix correction is applied (Figure 8c), but

good matches to core measurements are established when the maximum matrix correction was applied to the clay-corrected neutron porosity by using equation (14) (Figure 8d).

Among the 45 cored wells, 20 cored wells have both sonic and bulk density logs, which were used to calculate density-sonic porosity with equation (15). Figure 9a illustrates a comparison between measured core porosity and calculated density-sonic porosity. A total of 21 cored wells with both neutron and density logs were available to calculate neutron-density porosity with equation (16). A comparison between measured and calculated neutron-density porosities is shown in Figure 9b.

Type 2: Core-based model

Direct determination of porosity by core analysis is used to calibrate indirect measurements (such as density and sonic logs), which allows leveraging of limited core data to provide more information on areal and vertical variations in porosity.

Among 1026 core samples from 45 cored wells in the Viewfield area, more than 81% are from Unit A. From these, 619 and 359 samples are corresponded to sonic log and bulk density log values, respectively. They are used to establish equations to calculate porosity when a core sample is not available. However, there are not enough core samples for units B and C to provide a quantitative relationship between core porosity, sonic log or density log readings.

Core-Sonic log porosity model

Figure 10a shows a plot of measured core porosity versus sonic log values for all the samples in Unit A of the Middle Bakken Member. Most of the samples have porosity ranging from 5 to 15% and sonic transit-time ranging from 210 to 250 μs/m. Two quantitative relationships (linear and non-linear) between core porosity and sonic log indicate general trends of increasing sonic transit time with porosity. The relationships are expressed by the following equations:

$$PHIS2 = 2.1415 * 10^{-1} \Delta t - 37.9601 \quad (17a)$$

$$PHIS2 = - 4.0166 * 10^{-3} \Delta t^2 + 2.0379 \Delta t - 244.7855 \quad (17b)$$

where PHIS2 is the core-based sonic porosity using linear equation (17a) or non-linear equation (17b), in percentage; Δt is the sonic log reading. The polynomial equation (17b) seems to provide

a better sonic porosity calculation for the porosity range from 4 to 12%, but the linear equation (17a) gives better sonic porosity estimates when porosity is greater than 12%.

Core-Density log porosity model

Figure 10b shows a quantitative relationship between measured core porosity and bulk density log values as follows:

$$PHID2 = -3.2763 * 10^{-2} \rho_b + 94.2668 \quad (18)$$

where PHID2 is density porosity derived from a core-based model, in percentage; ρ_b is the bulk density log reading.

Comparison of results from proposed models with measured core porosity

Figure 11 shows the comparison of measured core porosity with calculated porosities using a conventional log-based volume model and core-based model for the Middle Bakken Member in the study area. For each well, track 1 shows the lithology logs, including gamma ray and spontaneous potential logs, and track 2 illustrates measures of core porosity (red dots) and seven calculated porosities using proposed equations (7), (10), (14), (15), (16), (17a)/(17b) and (18). The computed porosity curves include: (1) three porosity values from single log-based volume models, including density, sonic and neutron porosity; (2) density-sonic porosity and neutron-density porosities from dual-log volume model; and (3) single density porosity and sonic porosity from core-based models.

For Unit A of the Middle Bakken Member, coloured yellow in Figure 11, all the computed porosities show similar trends and values except in the intervals close to the top and base. Overall, the computed density porosity (PHID1) from the log-based volume model generally matches the measured core porosity best. The next preferred method is the neutron-density volume model (PHND), which gives porosity values that show a good match to the core measurements. The sonic porosities derived from the core-based model (PHIS2) match the core measurements very well except for the interval with porosity values higher than 15% in well 121/03-03-010-07W2. Calculated density porosities from the core-based model (PHID2) are very close to the measured core porosities for the upper interval of Unit A, but are slightly lower for the lower intervals that are dominated by siltstone. For most of the intervals in the selected wells, computed neutron (PHIN) and density-sonic porosities from volume models (PHDS) are

close to the measured core porosities. Computed porosity values from the single sonic log-based volume model (PHIS1) are slightly higher than core porosity measurements for some intervals or wells.

However, for Unit C of the Middle Bakken Member (coloured pink in Figure 11), the density porosity curve is obtained from volume model using equation (7) (PHID1). Obviously, calculated porosity derived from the density volume model is mainly lower than measured core porosity. A similar trend is also observed for Unit B. The calculation result indicates that the existing pyrite significantly affects density porosity even though the core grain density correction is applied. In this situation, the single density method is not recommended for use in determining reservoir porosity for Unit C or Unit B.

Permeability estimation

Core permeability model

As one of the main sources of understanding permeability distribution for each selected reservoir, direct measurement of permeability from core plugs is the most reliable method. However, the cores available do not cover the whole reservoir interval or all wells. In order to predict permeability in uncored intervals and wells, measured core porosity and permeability data is correlated and analyzed.

In this study, a total of 441 core samples with both measured porosity and permeability for Unit A from 21 wells were used to establish an empirical relationship between core porosity and core permeability (Figure 12a). The 21 wells, whose locations are distributed throughout the study area, are represented by red dots on Figures 12b and 2. A trend between core permeability and porosity has been observed for the selected core samples, and a linear equation at semi-logarithm axis has been obtained based on regression analysis and the correlation coefficient is 0.8182.

$$K_{CORE} = 1.5321*10^{-3}e^{0.3971\,\phi} \qquad (19)$$

where K_{CORE} is the core maximum permeability, in mD; ϕ is core porosity, in percentage.

The core porosity varies from 5% to 14.8% and the maximum permeability of the cores ranges from 0.01 to 1 mD (Figure 12a). The minimum permeability value of 0.01 mD may be due to the limit of measure for this parameter.

NMR permeability

As an advanced logging set, nuclear magnetic resonance (NMR) logging measures the induced magnetic moment of hydrogen nuclei (protons) contained within the fluid-filled pore space of porous media (reservoir rocks). Unlike conventional logging measurements (e.g., acoustic, density, neutron, and resistivity) that respond to both the rock matrix and fluid properties and are strongly dependent on mineralogy, NMR-logging measurements respond only to the presence of hydrogen. Because these protons primarily occur in pore fluids, NMR effectively responds to the volume, composition, viscosity, and distribution of fluids, such as oil, gas and water. The basic applications of NMR logging were aimed at providing important information on reservoir properties, such as lithology-independent total porosity, free and bound fluid porosity and permeability (Coates et al., 1999; Kleinberg, 2001).

The high-resolution combinable magnetic resonance tool (CMR-Plus) was introduced to enhance the precision of NMR logging (Schlumberger, 1995). The CMR-Plus tool provides not only lithology-independent porosity, free and bound fluid porosities, but also permeability curves with depth, including permeability computed using the Schlumberger-Doll-Research (SDR) model - K_{SDR} and the Timur-Coates equation - K_{TIM} (Kenyon et al., 1988).

In the Viewfield area, CMR-Plus enhanced NMR logging was performed for the Middle Bakken Members only in three wells (marked by blue triangles in Figures 2 and 12). The logging was used to acquire total NMR porosity (TCMR), effective NMR porosity (CMRP), NMR free fluid porosity (CMFF), NMR bound fluid porosity (BFV, if available), and NMR permeability curves (K_{TIM} and K_{SDR}). The results are shown in Figure 13 where 5 tracks are presented.

- Track 1 shows the basic lithology log set including gamma ray (GR) or spectral gamma ray (SGR), formation uranium concentration (HURA, if available), spontaneous potential (SP), and caliper log (HCAL);
- Track 2 shows three conventional porosity logs including compensated sonic transit time (DT, if available), bulk density (RHOB), photoelectric absorption factor (PEF), and neutron porosity (PHIN);
- Track 3 displays deep, medium and shallow resistivity curves (RD, RM and RS, respectively);

- Track 4 contains measured core porosity (PHI_{CORE}, the red dots) and NMR porosities that include total porosity (TCMR), effective porosity (CMRP), free fluid porosity (CMFF) and bound fluid porosity (BFV, if available); and
- Track 5 contains NMR permeability logs (K_{TIM} and K_{SDR}) and measured core maximum permeability (K_{MAX}, the blue dots).

Generally most of the total CMR porosity (TCMR) values exhibit close matches to the measured core porosity for most of the Middle Bakken Member in the three wells with NMR log set (Figure 13a, b and c). A big difference occurs between TCMR porosity and core measurements for a section in well 111/04-16-010-08W2, and this is probably because the TCMR measurement was affected by borehole rugosity and washout (Figure 13a), as indicated by the caliper log and the difference between caliper and borehole size (in the pink coloured area) in track 1 and track 4. CMR total porosity (TCMR) and effective porosity (CMRP) values are close for the Middle Bakken Member.

It is observed in Figure 13c that NMR permeability curves (K_{TIM} and K_{SDR}) show a similar trend to core permeability variation with depth for Unit A in well 111/01-17-008-06W2. However, differences are observed between K_{TIM} and K_{SDR} for well 131/08-03-008-08W2 (green coloured areas in Figure 13b), illustrating that K_{SDR} is higher than core measurements for some points for the upper interval of Unit A, and K_{TIM} is too low compared with measured core permeability for the lower interval of Unit A. Furthermore, significant differences occur between NMR permeability values (both K_{TIM} and K_{SDR}) and core permeability measurements for well 111/04-16-010-08W2 (Figure 13a), probably resulting from higher porosity caused by poor borehole conditions (rugosity and washout).

NMR permeability values, K_{SDR} and K_{TIM} versus TCMR porosity are plotted in semi-log axis for Unit A of the Middle Bakken Member (Figure 14). Excluding the data points in well 111/04-16-010-08W2 (Figure 13a), a good linear relationship is obtained for K_{SDR} versus TCMR:

$$K_{SDR} = 9.6609*10^{-5}\, e^{0.7352\phi} \qquad (20)$$

where K_{SDR} is the NMR permeability log from the Schlumberger-Doll-Research (SDR) model, ϕ is total CMR porosity (TCMR), in percentage.

Similarly, a non-linear relationship for K_{TIM} versus TCMR is obtained at semi-log axis:

$$K_{TIM} = 3.2834*10^{-12}\, \phi^{10.3136} \qquad (21)$$

where K_{TIM} is the NMR permeability log using the Timur-Coates equation.

Obviously, K_{SDR} is mostly higher than K_{TIM} at the same porosity. At lower porosity (<9%) and permeability (<0.01 mD), K_{TIM} is much lower than K_{SDR}. However, the difference decreases with increasing porosity. In a comparison with core measurements, K_{SDR} is a more reasonable match to measured values than K_{TIM}.

Figure 15 shows a comparison of two permeability models. In Figure 15a, two relationships are illustrated between permeability and porosity from core analysis and NMR log interpretation. Obviously, the two data sets overlap in a large area where the permeability is greater than 0.01mD (yellow coloured area). However, NMR data provides more detailed permeability variation in low permeability zones (<0.01mD) where porosity ranges from 5 to 7% (in the blue coloured area in Figure 15a). In contrast, the measured permeability values from some core samples are clustered at 0.01 mD against a porosity range of 5 - 8% due to the limit of permeability measurement (Figure 15a). In comparison with the permeability from a core-based model (K_{CORE}), the NMR permeability value (K_{SDR}) is mainly lower in a lower porosity zone ($\phi \leq 8.5\%$), but it is predominantly higher in higher porosity zones ($\phi > 10.5\%$), as shown in Figure 15a.

These two groups of data points are combined (the points are excluded in the green coloured area in Figure 15a); fair linear and non-linear relationships in the semi-log axis are established between porosity and permeability (Figure 15b).

$$K_{COM} = 1.0665*10^{-3}\, e^{0.4371\phi} \quad (22)$$

$$K_{COM} = 8.3995*10^{-6}\, \phi^{4.048} \quad (23)$$

where K_{COM} is permeability from the core-NMR model using the linear equation (22) or the non-linear equation (23), in mD. ϕ is core porosity or NMR porosity log data, in percentage.

The correlation coefficients of the linear equation (22) and non-linear equation (23) are 0.8263 and 0.8226 respectively, which are even higher than that of the core-based model – equation (19). Figure 15b illustrates that the combined dataset has a larger variation both in porosity and maximum permeability, ranging from 5 to 15%, and 0.001 to 2 mD, respectively.

In a low porosity zone ($\phi \leq 6.7\%$, the blue coloured area in Figure 15b), the K_{COM} non-linear equation (23) is suggested to be applied for permeability estimation since more detailed NMR data are used for regression. In a higher porosity zone ($6.7\% < \phi < 12.5\%$), both the linear equation

(22) and the non-linear equation give very close permeability estimates. However, a notable difference occurs between the permeability values from the two equations with increasing porosity from 12.5% (the orange coloured area in Figure 15b). In this situation, the better fitting linear equation (22) is preferred.

Figure 16 illustrates the calculation results from the proposed models in this study for Unit A of the Middle Bakken Member for the three wells with NMR logging set. Track 4 shows total NMR porosity log (TCMR), calculated density porosity (PHID1) derived from proposed bulk volume equation (7), and measured core porosity (PHI_{CORE}, the red dots). It is clear that computed porosity from the volume density model displays a better correlation with measured core porosity. Track 5 shows permeability curves, including core permeability measurements K_{MAX} (the blue dots), NMR permeability log K_{SDR} (the orange dashed line), calculated permeability K_{CORE} (the blue line) from the core-based permeability model - equation (19), and K_{COM} (the pink line) derived from core-NMR permeability model - equation (22) or (23), using calculated density porosity (PHID1). In general, both the core-based and core-NMR models produce reasonable permeability estimates (Figure 16), which better match the core permeability values than NMR permeability K_{SDR} (Figure 16a and b).

Correlations

Six stratigraphic cross sections, showing porosity and permeability determined by using the proposed log analysis methods, have been built for Unit A of the Middle Bakken Member in the Viewfield Pool. They are correlated to understand the thickness variations and the petrophysical parameter distributions along the cross sections.

Figure 17 shows the basic log-signatures and computed porosity (PHID1, if density log is available; or PHIS1 if only sonic log is available) using equation (7) and estimated permeability (K_{COM}) using core-NMR model for Unit A of the wells from south to north along cross section A-A' (the solid orange line in Figure 17). Log analysis indicates that the calculated average porosity value generally increases from south (A) toward north (A'), from 8.6% to 13.5%. Computed average maximum permeability also increases from less than 0.1 mD to over 0.75 mD along cross section A-A'. A decrease in thickness of Unit A is also shown along the cross section, from south to north.

Figure 18 illustrates the correlation result of porosity, permeability and thickness for cross section B-B'. It shows that the thickness of Unit A is greater than 9 m for each well in the cross section, ranging from 9 meters to 11 m. Log analysis indicates that most of the average porosity values of Unit A are greater than 10%, and the permeability values are higher than 0.1 mD, ranging from 0.12 mD to 0.45 mD. However, two wells (101/09-29-007-08W2 and 111/02-26-009-09W2) have lower porosity (<10%) and lower permeability (<0.1 mD).

Figure 19 displays the basic well logs and calculated petrophysical parameters for each well along cross section C-C', from south to north. Unit A exhibits variable thickness along the cross section, ranging from 6.6 m to over 10 m. Log analysis indicates that Unit A has good average porosity, mostly greater than 10%, and the average permeability values are dominantly greater than 0.11 mD, except in well 131/12-15-006-11W2, located at the south edge of cross section C-C'.

Cross section line D-D' is in the south part of the Viewfield Pool. In comparison with the wells in other cross sections, all the wells along cross section D-D' have thicker Unit A (9.6 m to 12.6 m) (Figure 20). Log analysis indicates that most of Unit A consists of thick (≥10 m) interbedded siltstone and sandstone. Computed average porosity values for Unit A range from 9% to 13%, and the average permeability values are between 0.1 mD and 0.45 mD for the nine wells along cross section D-D'.

Figure 21 shows that the thickness of Unit A ranges from 6 m to 9.4 m along cross section E-E'. Log analysis indicates that the average porosities for Unit A range from 9% to 13.4%, and the average permeability values are between 0.11 mD and 0.4 mD for the five wells in this cross section.

Figure 22 displays the correlation results along cross section F-F'. Log analysis indicates that the average porosity values for Unit A have a narrow range from 8.8% to 10.2% for the four wells on the western side of cross section F-F', and the average permeability values range from 0.06 mD to 0.12 mD. However, for the three wells on the eastern side of cross section F-F', the average porosity and permeability is between 12% and 13.8%, and 0.2 mD to 0.39 mD, respectively. The thickness of Unit A is variable but less than 9.5 m for all the wells in this cross section.

The well log estimated porosity and permeability shows general upward increasing trends in the wells on the six cross sections, which are consistent with the observation of coarsening gradually upward in Unit A from cores. This supports the inference that the majority of hydrocarbon production is from the upper part of the unit.

CONCLUSIONS AND DISCUSSION

This report describes the proposed petrophysical models in detail and their applications in reservoir characterization for the Viewfield Bakken play in southeastern Saskatchewan. A thorough analysis of core measurements illustrates the distribution of porosity and permeability for the Middle Bakken Member: 1) Unit B has the best porosity (an average of 11.1% and a median value of 11.8%) and highest permeability (an average of 4.55 mD); 2) Unit C has the lowest porosity (8.6% on average) and fair permeability values (1.87 mD on average); and 3) Unit A has fair porosity values (10.4% on average) but the lowest average permeability (0.32 mD).

In the present study, two types of porosity models are presented: log-based bulk volume models and core-based models. The proposed bulk volume porosity model, with matrix parameter and clay corrections, has been used to establish 5 equations to calculate reservoir porosity using single-log sonic, density and neutron, and a dual-log of density-sonic and neutron-density for Unit A of the Middle Bakken Member in the Viewfield Pool. Among the three single-log porosity equations, the density volume equation gives the best match with measured core porosity. The computed porosity from single sonic and neutron logs match the core measurements fairly well, and thus give reasonable porosity estimates. Dual-log volume equations of neutron-density and density-sonic also provide good results when compared with core measurements. The core-based model has been used to generate single-log density and sonic equations that also provide comparable alternative porosity calculations for the study area. Both porosities derived from density model (PHID1) and the NMR logging tool (TCMR) are close to core measurements in intervals with good borehole conditions. Where the borehole is enlarged, TCMR overestimates the porosity due to increased hydrogen index from mud. In this case, density porosity matches better with measured core porosity.

In addition to porosity models, core-based and core-NMR permeability models are proposed, which provide reasonable permeability estimates for Unit A of the Middle Bakken Member and are comparable with core measurements.

The proposed methods are used to compute porosity and permeability for Unit A within the Middle Bakken Member in wells on the six cross sections, to display reservoir heterogeneity in the Viewfield play. The results are supported by core observations and measurements.

The matrix correction for the volume porosity models was based on the assumption of very little pyrite content existing in Unit A for this study. However, pyrite content in the reservoir varies across the study area and therefore sonic, neutron and neutron-density methods provide better reservoir porosity estimation when a higher amount of pyrite is present in Unit A.

For units B and C, calculated porosity using a single density volume model may underestimate the porosity value since variable amounts of pyrite significantly affect the density log readings. Further research is required to develop models applicable to units B and C of the Middle Bakken Member.

ACKNOWLEDGEMENTS

The authors would like to thank Heather Brown and Dr. Denis Jiang for their comprehensive reviews and edits of this report. We also thank Saskatchewan Ministry of the Economy for providing basic well information and core analysis data. This work is supported by the Shale Petroleum Resources Assessment project under the Geoscience for New Energy Supply (GNES) program of the Geological Survey of Canada.

REFERENCES

Angulo, S. and Buatois, L.A., 2011. Integrating depositional models, ichnology, and sequence stratigraphy in reservoir characterization: The Middle Member of the Devonian-Carboniferous Bakken Formation of subsurface southeastern Saskatchewan revisited, AAPG Bulletin, V.96, No.6, pp1017-1043.

Christopher, J.E., 1961. Transitional Devonian-Mississippian Formations of Southern Saskatchewan; Saskatchewan Department of Mineral Resources, Report 66, 103p.

Coates, G.R., Xiao, L., and Prammer, M.G, 1999. NMR Logging Principles and Applications. Halliburton Energy Services, Houston, USA.

Cronkwright, D.J., Pedersen, P.K., and Spencer, R.J., 2014. Detailed reservoir characterization of the Middle Member Bakken Formation – Viewfield Pool, SE Saskatchewan, CSPG Convention 2014.

Hu, K., Chen, Z., and Yang, C., 2015. Petrophysical analysis of reservoir characterization for the Devonian-Mississippian Lower Middle Bakken Member in the Viewfield Pool, SE Saskatchewan, CSPG GeoConvention 2015.

Kenyon, W.E., Day, P.I., Straley, C. et al., 1988. A three-part study of NMR longitudinal relaxation properties of water-saturated sandstones. SPE Form Eval 3 (3): 622–636. SPE-15643-PA.

Kleinberg, R.L., 2001. Part 4 - NMR Well Logging at Schlumberger, Concepts in Magnetic Resonance, Vol. 13(6), pp396-403.

Kohlruss, D. and Nickel, E., 2009. Facies analysis of the Upper Devonian-Lower Mississippian Bakken Formation, southeastern Saskatchewan; *in* Summary of Investigations 2009, Volume 1, Saskatchewan Geological Survey, Saskatchewan Ministry of Energy and Resources, Miscellaneous Report 2009-4.1, Paper A-6, 11p.

Kohlruss, D. and Nickel, E., 2012. Understanding Saskatchewan's Middle Bakken Oil Trapping Mechanisms, CSPG GeoConvention 2012.

Kohlruss, D. and Nickel, E., 2013. Bakken Formation of southeastern Saskatchewan – selected stratigraphy and production maps; Saskatchewan Ministry of the Economy, Saskatchewan Geological Survey, Open File 2013-1, one sheet with marginal notes.

Kohlruss, D., McLeod, J., and Nickel, E., 2013. Well stimulation observations in the Viewfield Bakken Pool - What is the production telling us? Williston Basin Petroleum Conference 2013.

Kreis, L.K., Costa, A.L., and Osadetz, K.G., 2006. Hydrocarbon potential of Bakken and Torquay formations, southeastern Saskatchewan; *in* Gilboy, C.F. and Whittaker, S.G. (eds.),

Saskatchewan and Northern Plains Oil & Gas Symposium 2006, Saskatchewan Geological Society, Special Publication 19, p118-137.

Schlumberger, 1989. Log Interpretation Principles/Applications.

Schlumberger, 1995. CMR-Plus Combinable Magnetic Resonance Tool. www.slb.com

Staruiala, A., Qing, H., and Chi, G., 2013. Preliminary analysis of lithology and facies in the Bakken Formation, southeastern Saskatchewan, Canada; *in* Summary of Investigations 2012, Volume 1, Saskatchewan Geological Survey, Saskatchewan Ministry of Energy and Resources, Miscellaneous Report 2012-4.1, Paper A-6, 9p.

Wyllie, M.R.J., Gregory, A.R., and Gardner, L.W., 1956. Elastic Wave Velocities in Heterogeneous and Porous Media. Geophysics 21 (1), p41–70. http://dx.doi.org/10.1190/1.1438217

Zhao, Y. and Qing, H., 2014. Petrophysical properties of the tight Bakken reservoirs, Southern Saskatchewan, Canada. GeoConvention 2014 focus, CSPG, 2014.

LIST OF FIGURES

14. NMR permeability K_{SDR} computed using Schlumberger-Doll-Research (SDR) and K_{TIM} using Timur-Coates model from two wells 131/08-008-08W2, and 111/01-17-008-06W2, as shown in Figures 13(b) and (c), respectively. Good quantitative relationships are obtained between K_{SDR}, K_{TIM} and TCMR at semi-logarithm axis for Unit A of the Middle Member of the Bakken Formation in the Viewfield Pool.

15. Comparison of permeability models for Unit A of the Middle Bakken Member in the Viewfield Pool. (a) Two relationships, K_{CORE} equation (19), and K_{SDR} equation (20), between permeability and porosity from core analysis and advanced NMR log interpretation. (b) Relationships between permeability and porosity from combined dataset from core analysis from 21 wells and most of K_{SDR}-TCMR data pairs from two wells, including linear equation (22) and on-linear equation (23) at semi-logarithm axis.

16. Examples showing a comparison of NMR porosity and permeability with calculated porosity and permeability derived from proposed porosity and permeability models in this study for Unit A of the Middle Bakken Member for three wells 111/04-16-010-08W2 (a), 131/08-03-008-08W2 (b), and 111/01-17-008-06W2 (c) in the Viewfield Pool of southeastern Saskatchewan.

17. Stratigraphic cross section A-A' showing the basic log signature, calculated porosity and permeability for Unit A of the Middle Bakken Member. The top of the Upper Bakken Shale has been used as a stratigraphic datum, and the bottom of the Lower Bakken shale is the end depth of the correlation.

18. Stratigraphic cross section B-B' showing the basic log signature, calculated porosity and permeability for Unit A of the Middle Bakken Member. The top of the Upper Bakken Shale has been used as a stratigraphic datum, and the bottom of the Lower Bakken shale is the end depth of the correlation.

19. Stratigraphic cross section C-C' showing the basic log signature, calculated porosity and permeability for Unit A of the Middle Bakken Member. The top of the Upper Bakken Shale has been used as a stratigraphic datum, and the bottom of the Lower Bakken shale is the end depth of the correlation.

20. Stratigraphic cross section D-D' showing the basic log signature, calculated porosity and permeability for Unit A of the Middle Bakken Member. The top of the Upper Bakken Shale has been used as a stratigraphic datum, and the bottom of the Lower Bakken shale is the end depth of the correlation.

21. Stratigraphic cross section E-E' showing the basic log signature, calculated porosity and permeability for Unit A of the Middle Bakken Member. The top of the Upper Bakken Shale has been used as a stratigraphic datum, and the bottom of the Lower Bakken shale is the end depth of the correlation.

22. Stratigraphic cross section F-F' showing the basic log signature, calculated porosity and permeability for Unit A of the Middle Bakken Member. The top of the Upper Bakken Shale has been used as a stratigraphic datum, and the bottom of the Lower Bakken shale is the end depth of the correlation.

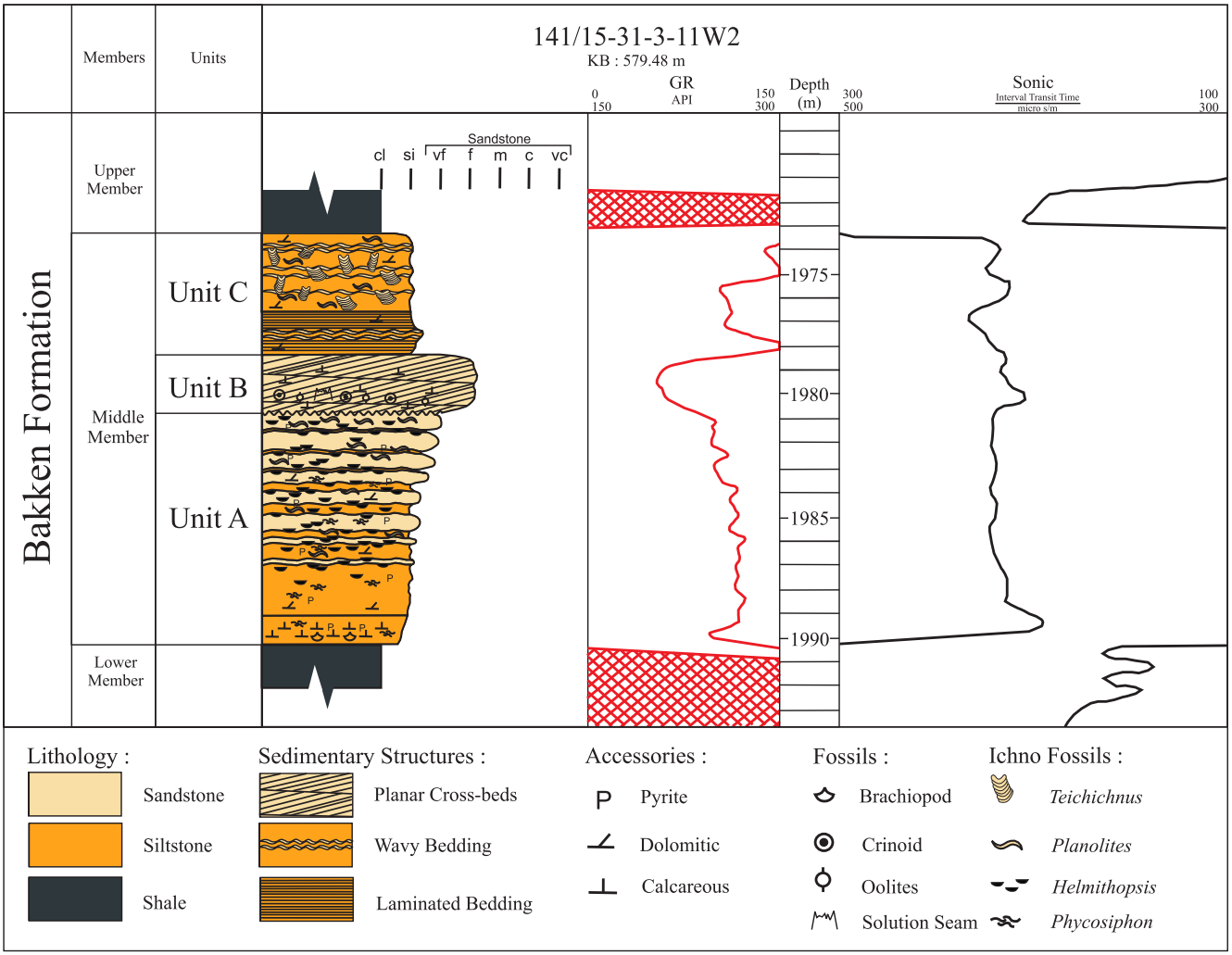

Figure 1. Core log of the Bakken Formation (based on well core 141/15-31-3-11W2) , showing its stratigraphic subdivisions, gamma ray and sonic transit time logs. Units A, B, and C of the Middle Bakken Member were classified using the parameters set from core and well logs (Kohlruss and Nickel, 2013).

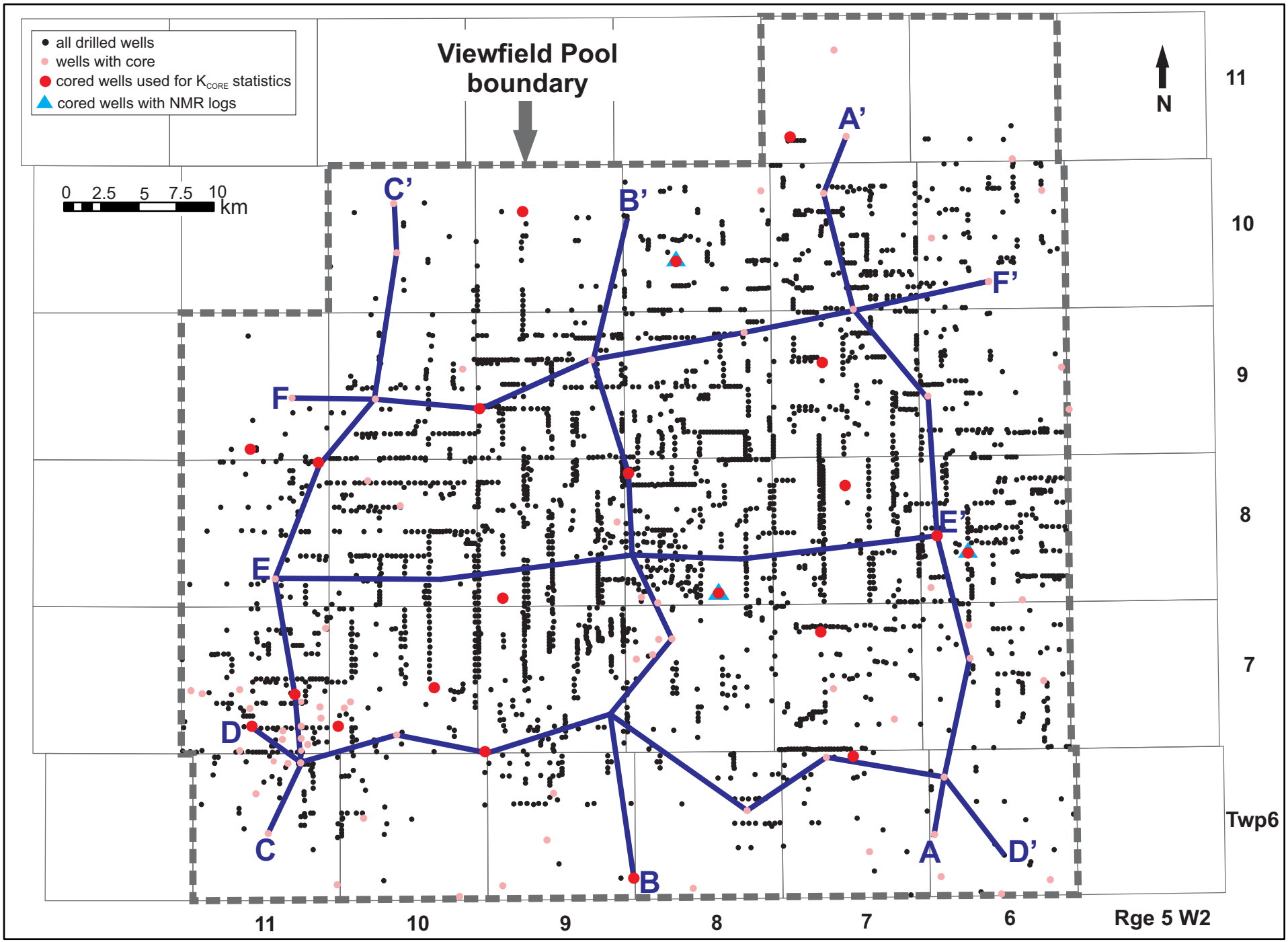

Figure 2. Map of the study area showing all wells and cross-section lines in the Viewfield Pool in southeastern Saskatchewan.

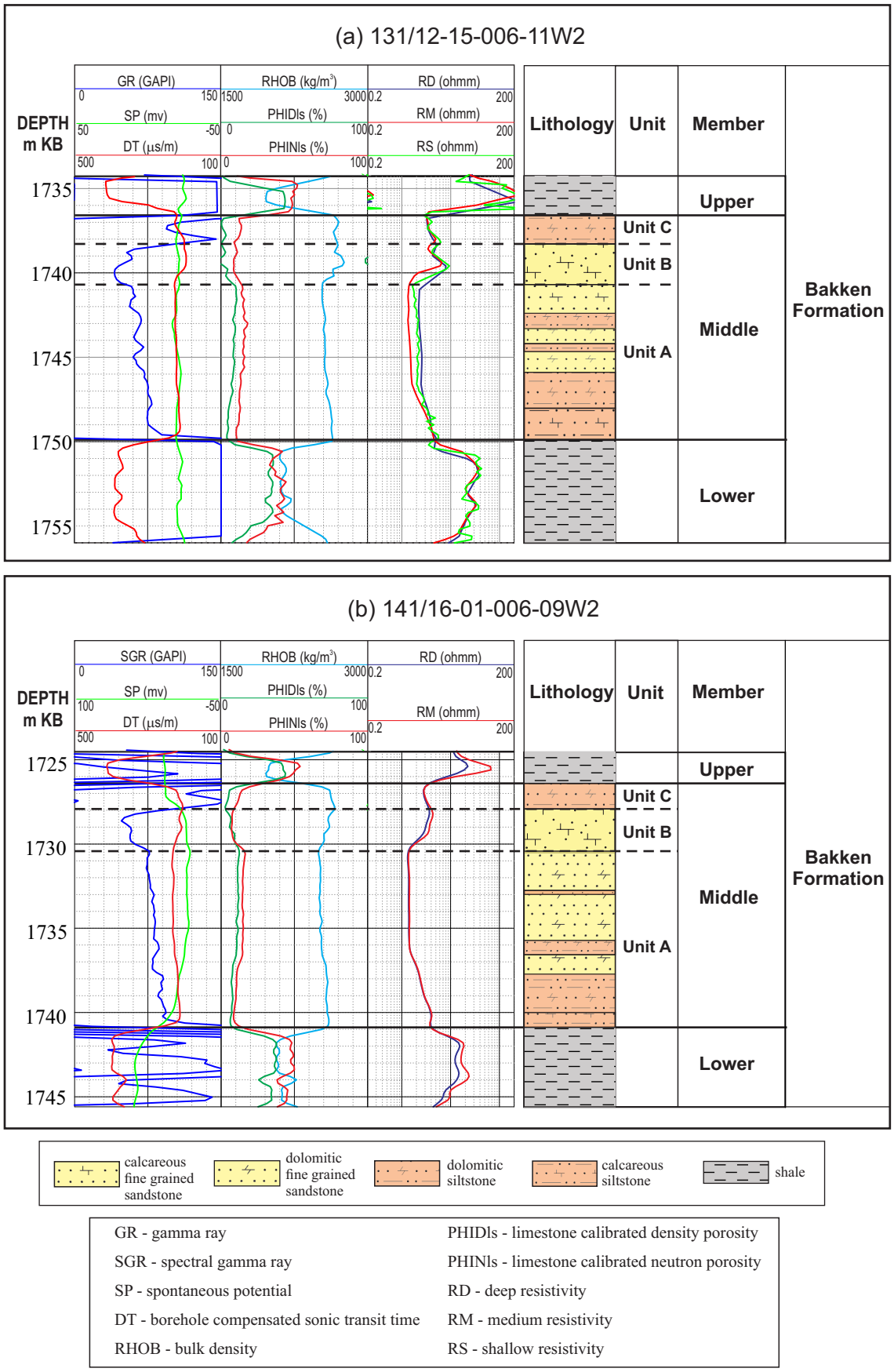

Figure 3. Examples from two wells showing log signatures for the Bakken Formation in the Viewfield Pool of Saskatchewan, including Upper Member (upper shale), Middle Member (Unit C, Unit B and Unit A) and Lower Member (lower shale). Units A, B and C, classified by Kohlruss and Nickel (2013), can be identified by using well logs.

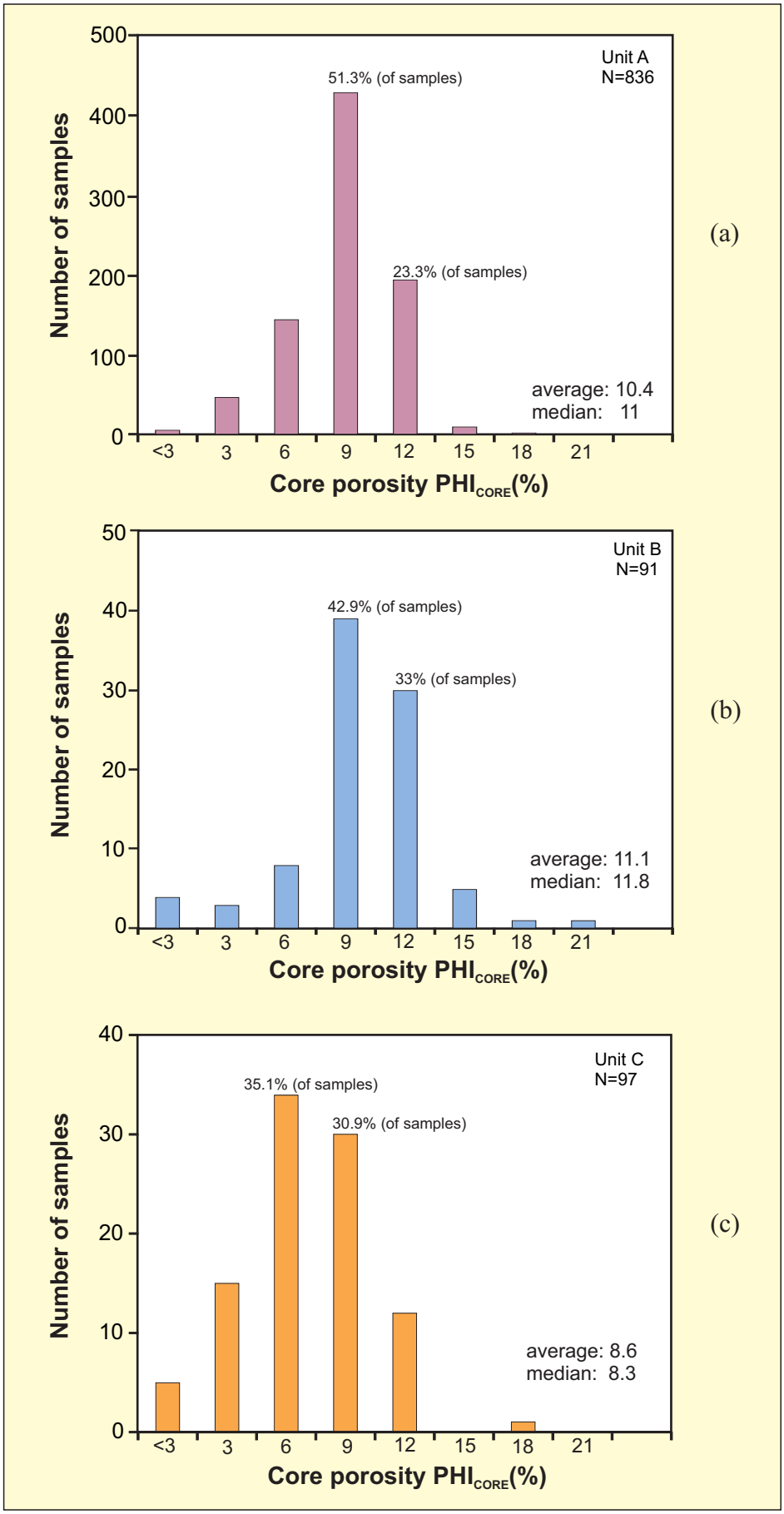

Figure 4. Core porosity (PHI_{CORE}) distribution for units A, B and C of the Middle Bakken Member in the Viewfield Pool, southeastern Saskatchewan. N: total number of samples.

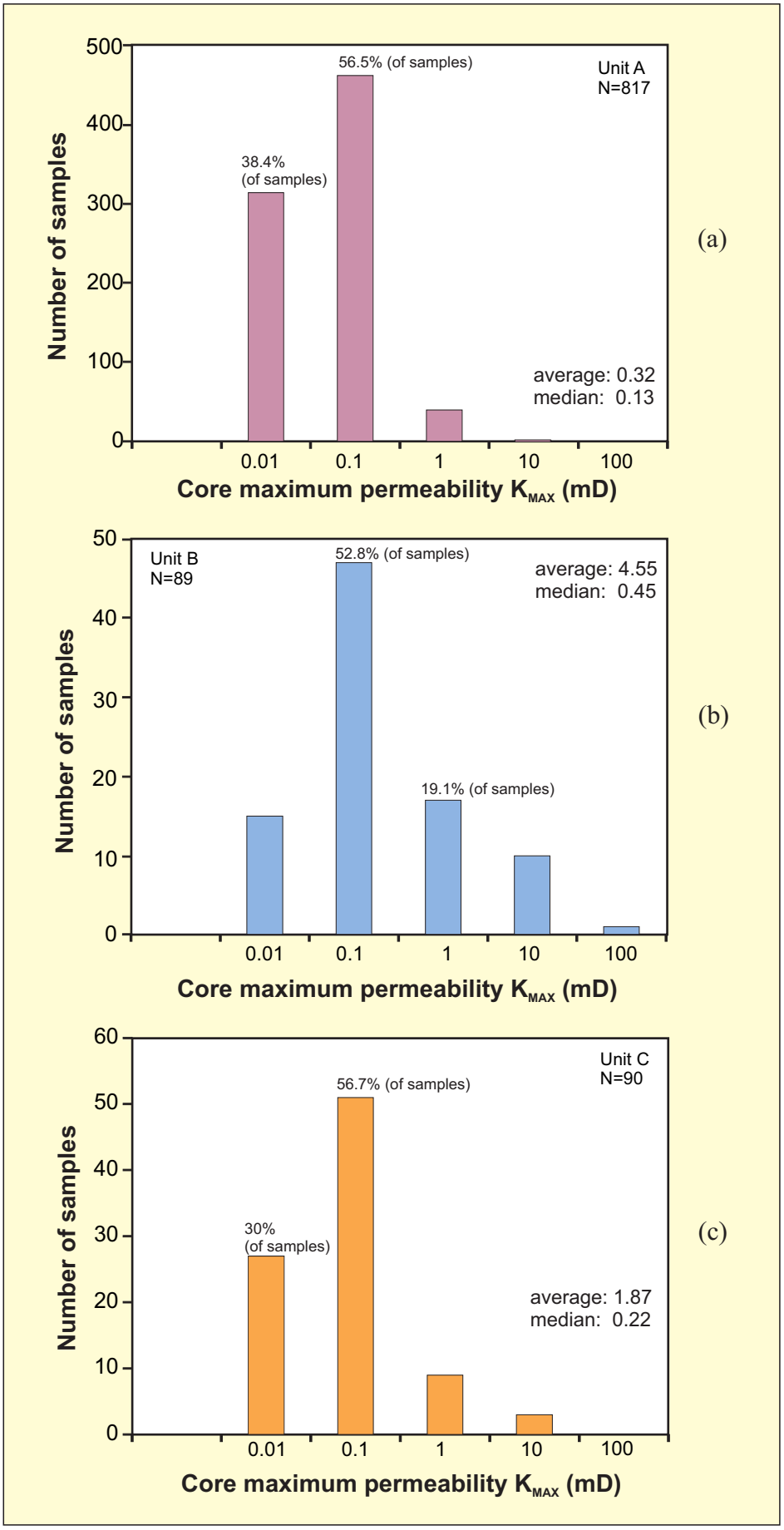

Figure 5. Core max permeability (K_{MAX}) distribution for units A, B and C of the Middle Bakken Member in the Viewfield Pool, southeastern Saskatchewan. N: total number of samples.

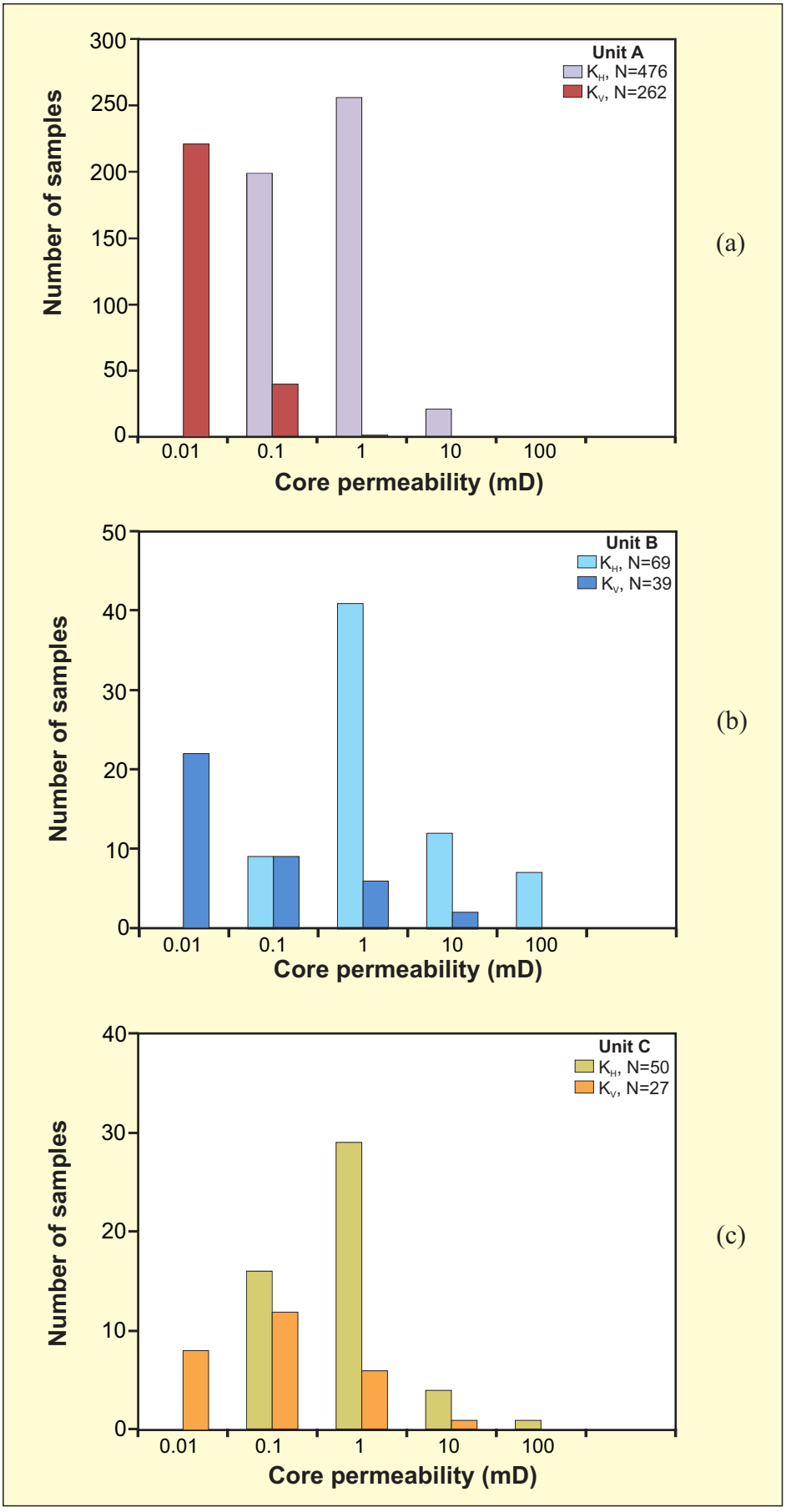

Figure 6. Core horizontal permeability (K_H) and vertical permeability (K_V) distribution for units A, B and C of the Middle Bakken Member in the Viewfield Pool, southeastern Saskatchewan. N: total number of samples.

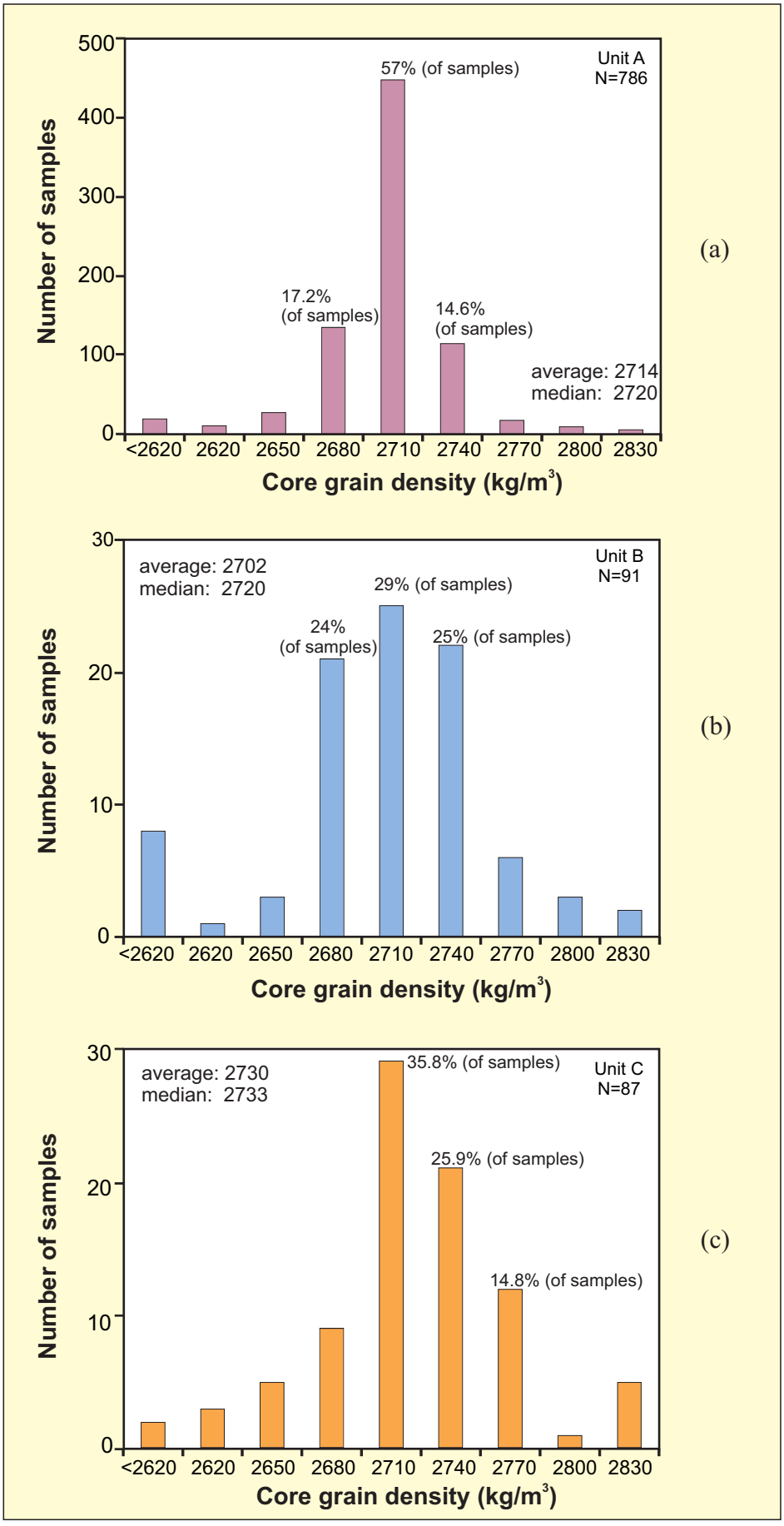

Figure 7. Core grain density distribution for units A, B and C of the Middle Bakken Member in the Viewfield Pool, southeastern Saskatchewan. N: total number of samples.

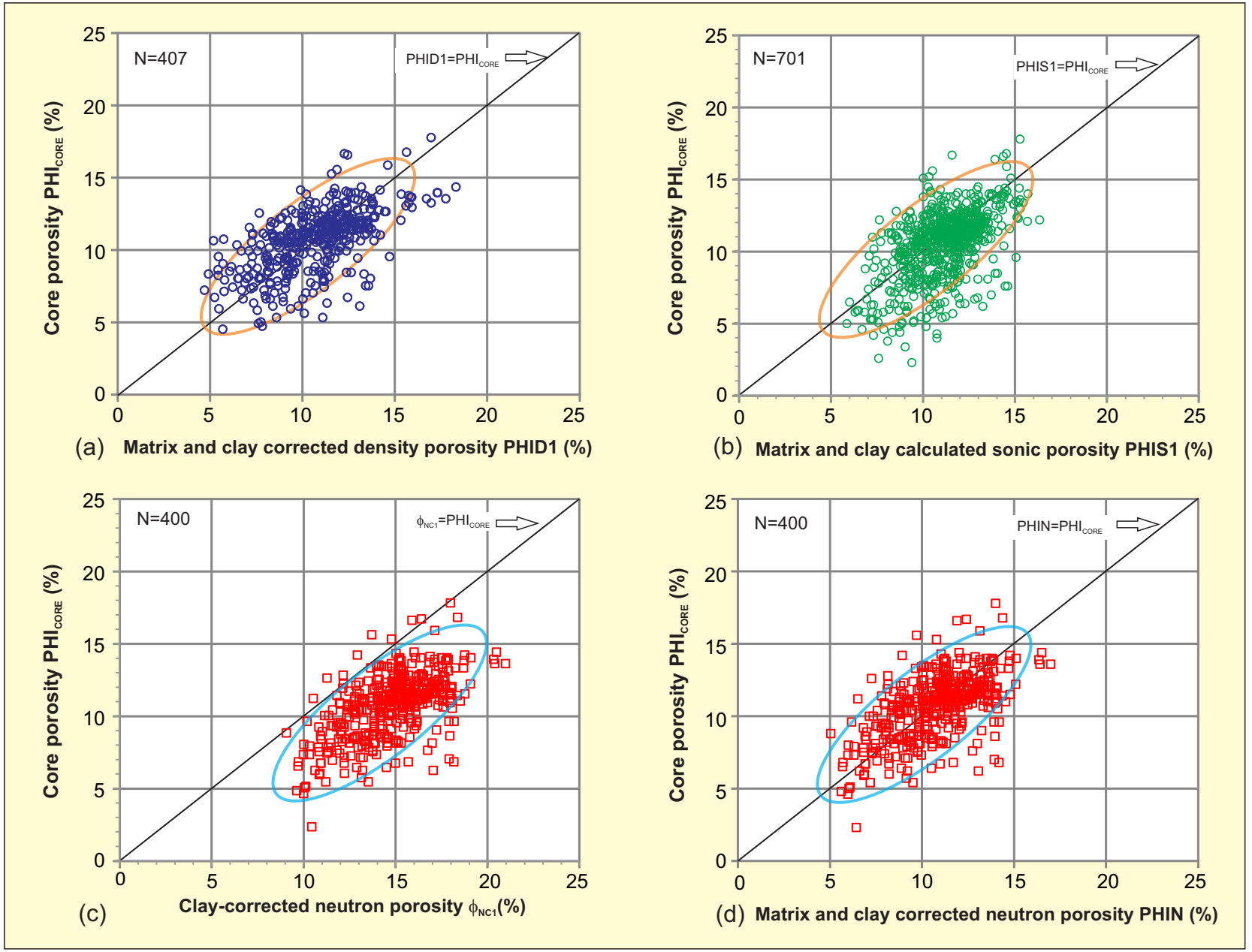

Figure 8. Comparison of measured core porosity (PHI_{CORE}) with calculated porosities from single porosity log for Unit A of Middle Bakken Member of Viewfield Pool, southeastern Saskatchewan. N: total number of samples.
(a) - matrix- and clay-corrected density porosity using equation (7),
(b) - matrix- and clay-corrected sonic porosity using equation (10),
(c) - clay-corrected neutron porosity (with limestone calibration) using equation (12),
(d) - matrix- and clay- corrected neutron porosity using equation (14).

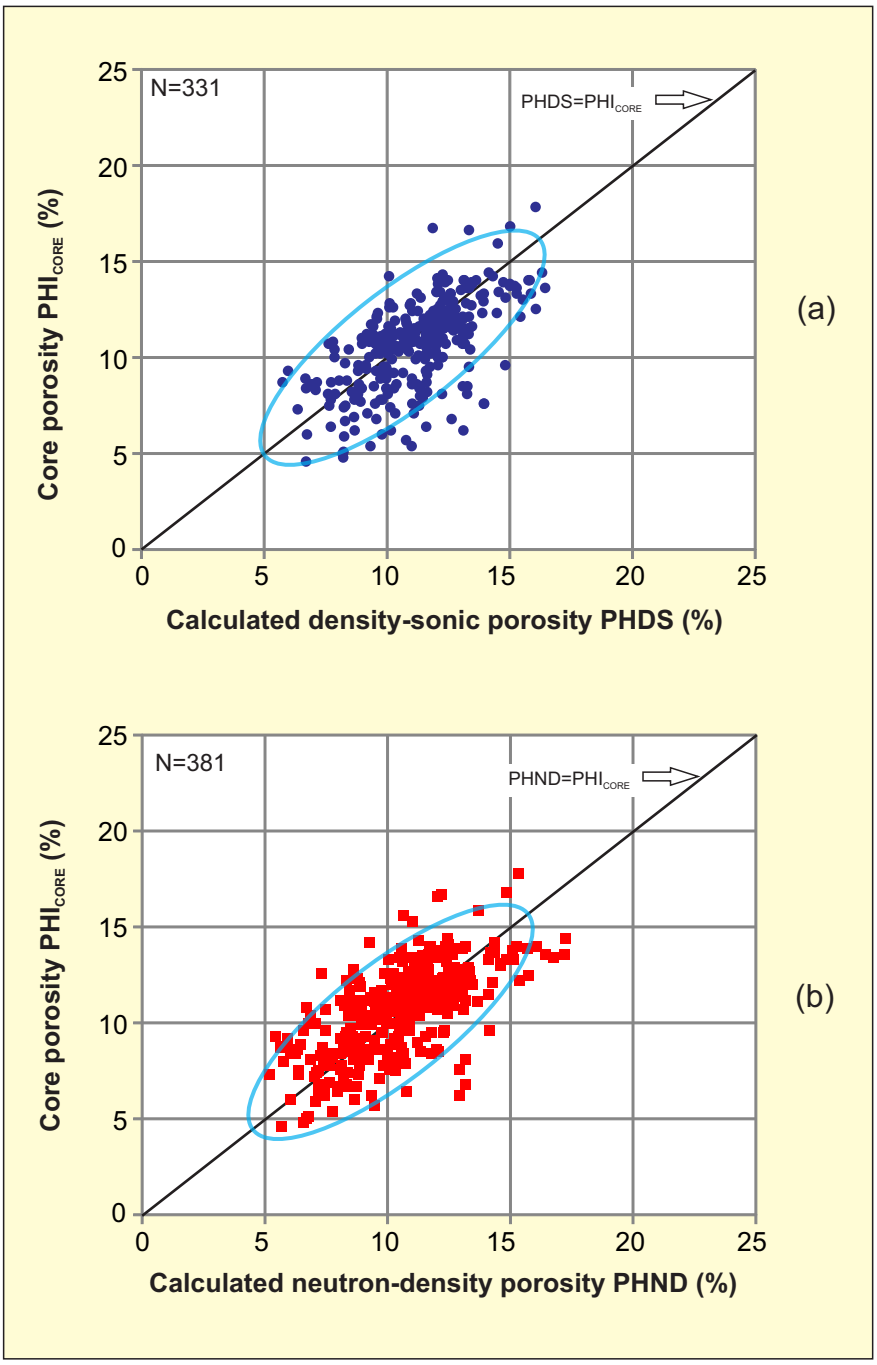

Figure 9. Comparison of dual-log calculated porosities with core porosity for Unit A of Middle Bakken Member in the Viewfield Pool, southeastern Saskatchewan. N: total number of samples. (a) - calculated density-sonic porosity using equation (15) versus measured core porosity, (b) - calculated neutron-density porosity using equation (16) versus measured core porosity.

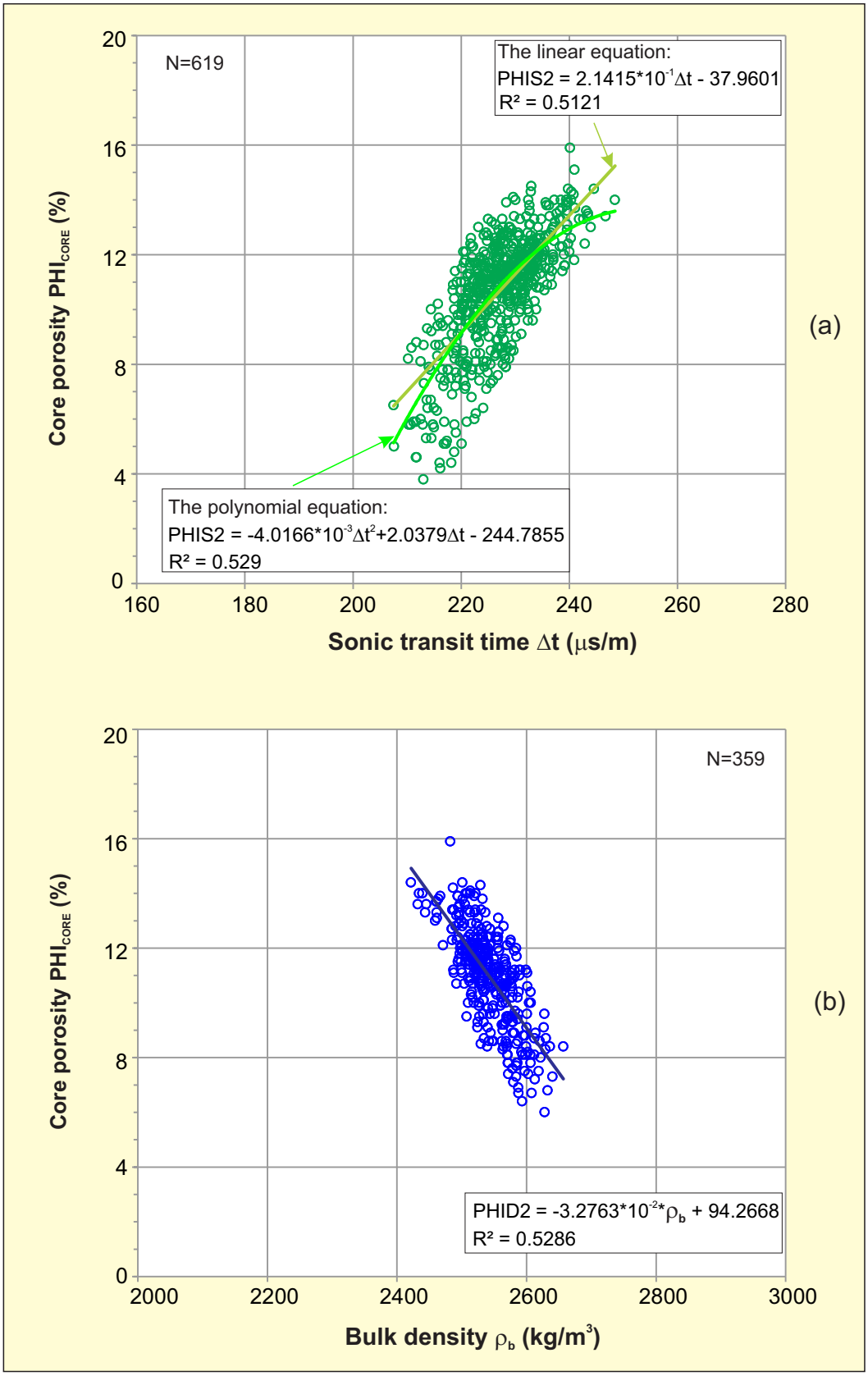

Figure 10. Quantitative relationships between measured core porosity and sonic transit time log (a), including linear equation and polynomial equation. Quantitative relationship between measured core porosity and bulk density log reading (b). All data are from Unit A of the Middle Bakken Member in the Viewfield Pool, southeastern Saskatchewan. N: total number of samples.

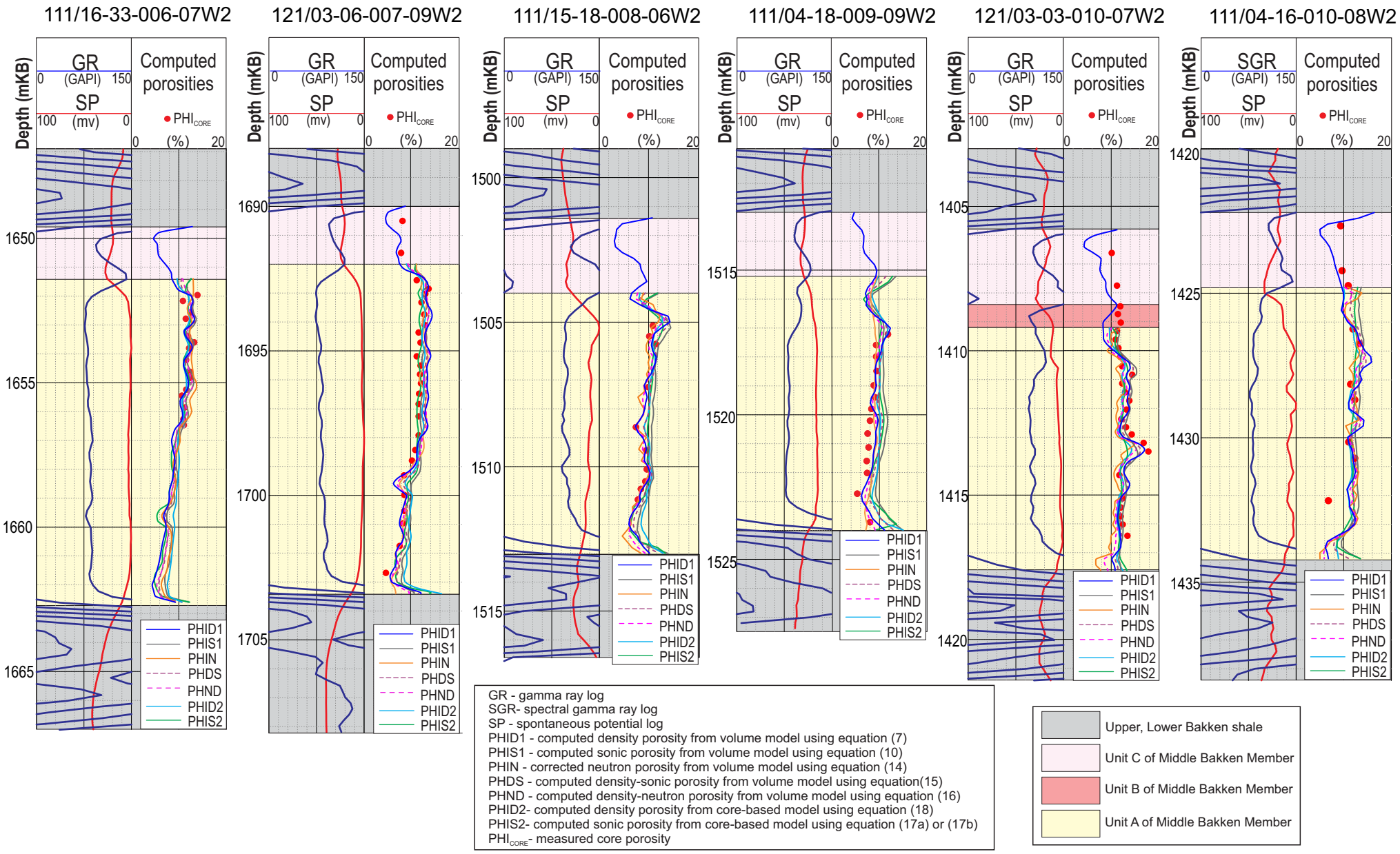

Figure 11. Examples showing comparison of computed porosities derived from proposed porosity models using wireline logs with core porosity measurements for the Middle Bakken Member in the Viewfield Pool, southeastern Saskatchewan.

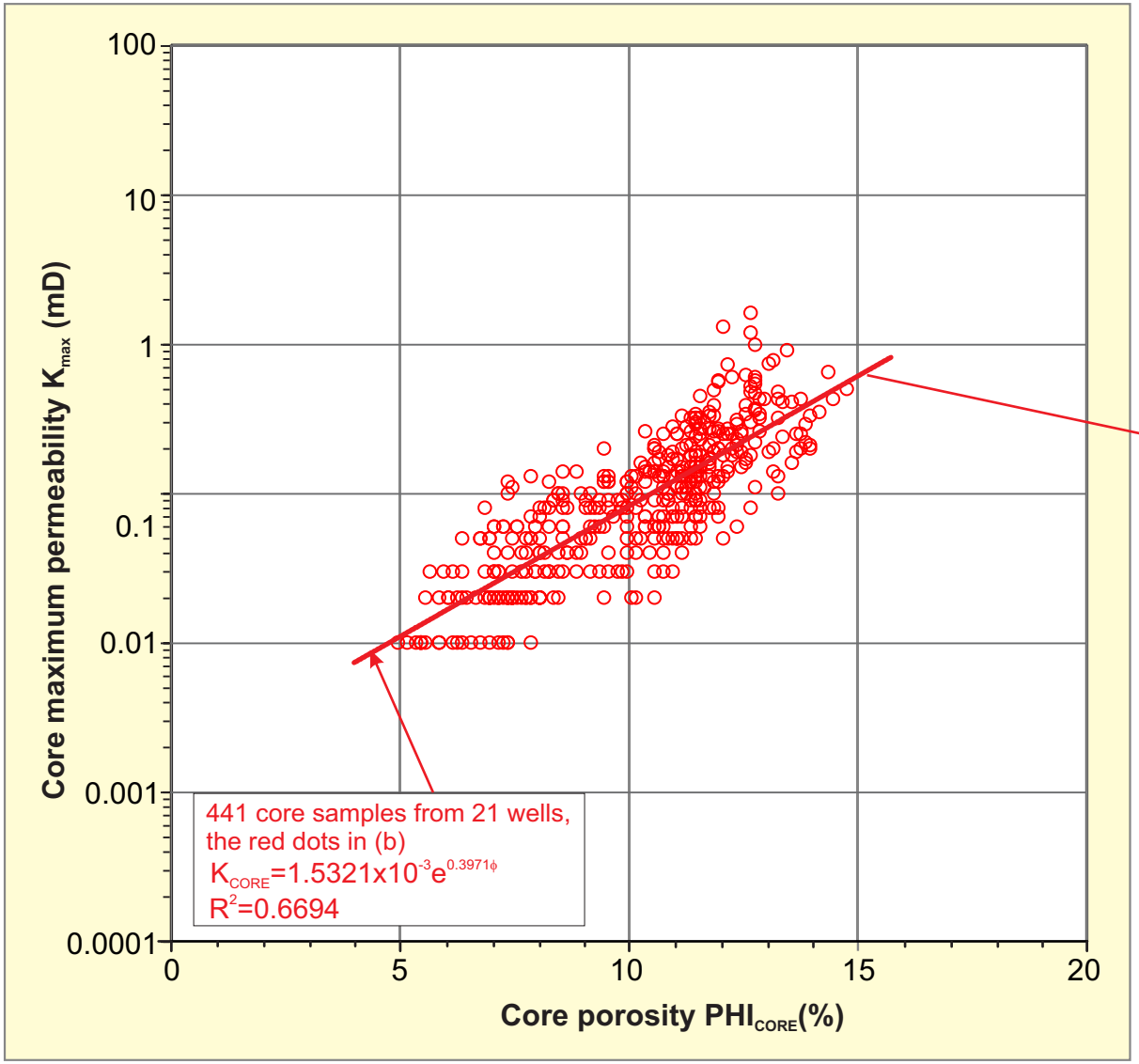

(a) Core porosity versus permeability

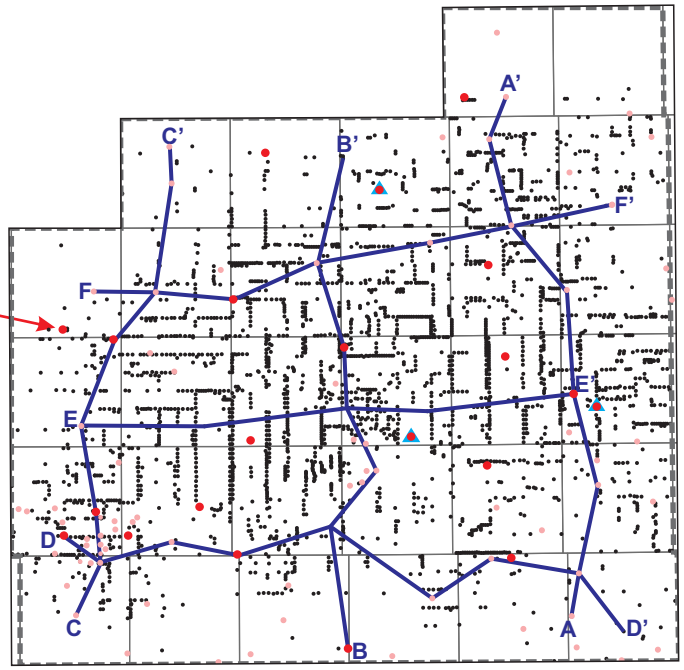

(b) Well locations in the Viewfield Pool. The red dots represent the 21 wells used for K_{CORE} equation statistics. The blue triangles stand for the three cored wells with NMR logging set.

Figure 12. Core maximum permeability (K_{max}) versus core porosity (PHI_{CORE}) for 21 selected wells for Unit A of the Middle Member of the Bakken Formation in the Viewfield Pool in southeastern Saskatchewan. Quantitative relationships between core permeability and porosity has been obtained based on regression analysis when several anomaly points with very high porosity (>15%) and permeability (>4 mD) were removed.

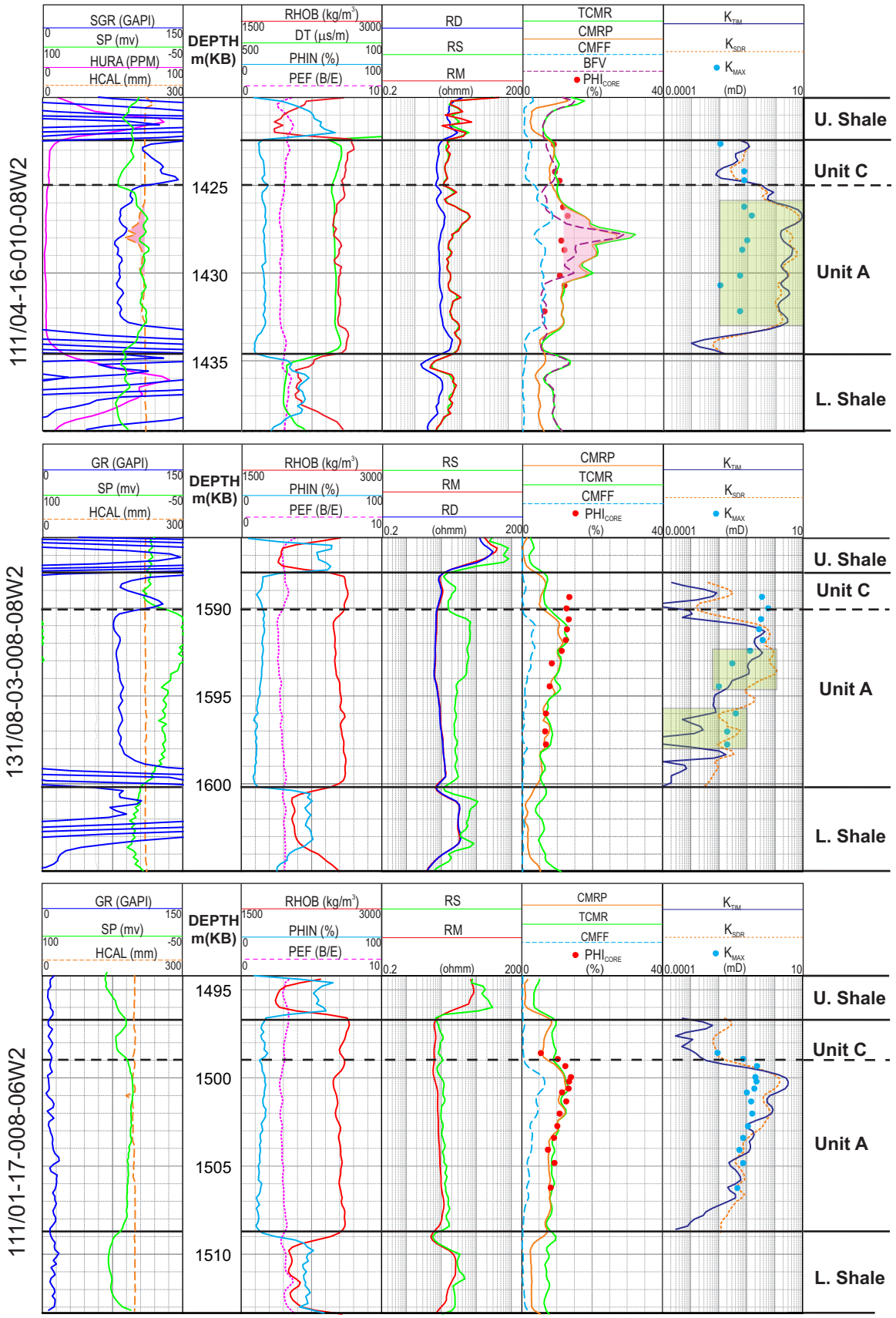

GR - gamma ray log
SGR- spectral gamma ray log
SP - spontaneous potential log
HURA- uranium concentration
HCAL- caliper

RHOB-density log
DT- sonic transit time log
PHIN- neutron porosity log
PEF- photoelectric factor
RD- deep resistivity log

RM- medium resistivity log
RS- shallow resistivity log
interval where difference occurs between NMR permeability and core measurements

TCMR- CMR porosity log
CMRP- effective NMR porosity
CMFF- NMR free fluid porosity
BFV- NMR bound fluid porosity
PHI_{CORE}- measured core porosity

K_{SDR}- NMR permeability from Schlumberger-Doll-Research (SDR) model
K_{TIM}- NMR permeability from Timur-Coates equation
K_{MAX}- measured core maximum permeability

Figure 13. Results of the complete log set that was run in wells 111/04-16-010-08W2 (a), 131/08-03-008-08W2 (b), and 111/01-17-008-06W2 (c) in the Viewfield Pool (blue triangles on Figure 2 and 12). Detailed porosity and permeability interpretations are displayed from NMR logging set for the Middle Member of the Bakken Formation in all three wells.

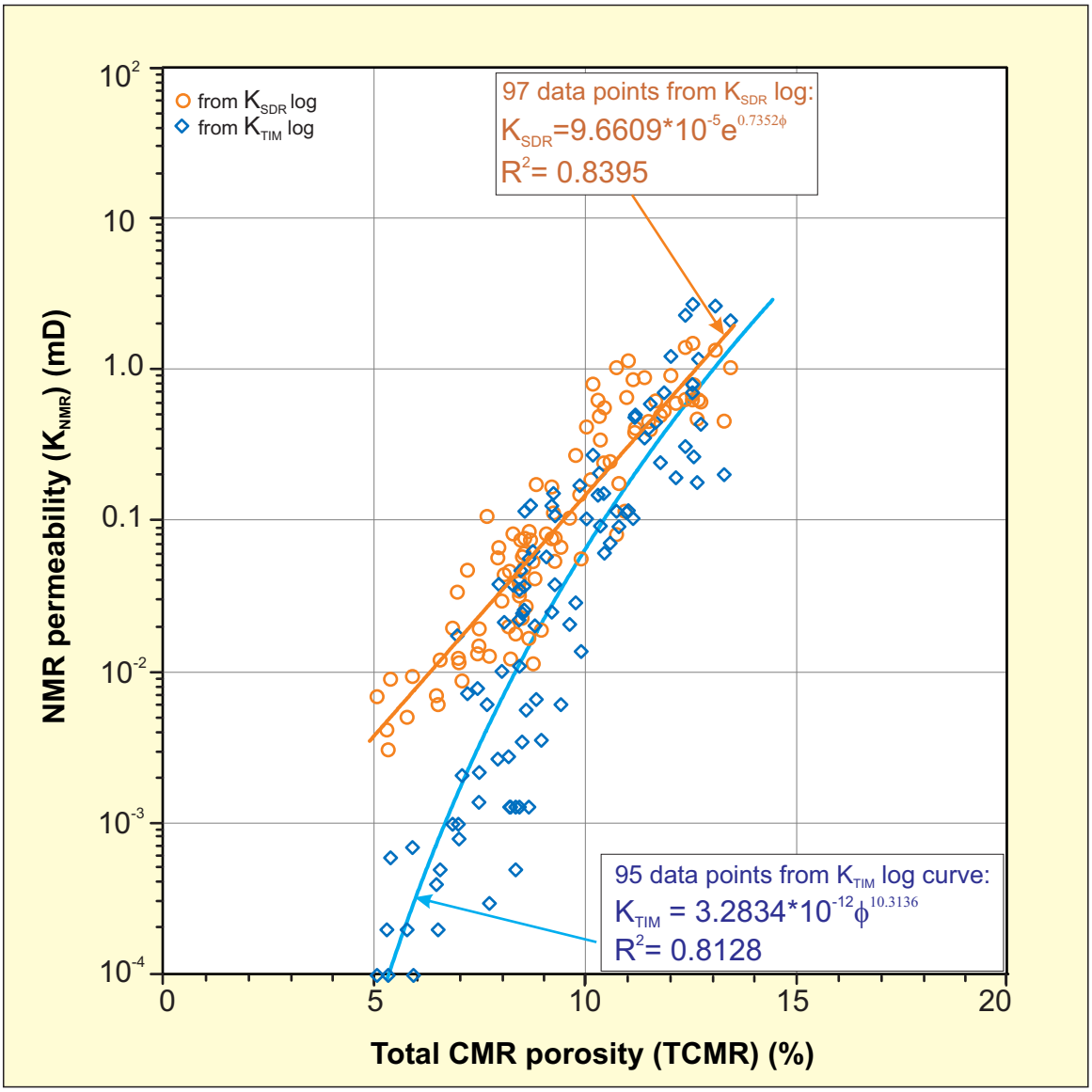

CMR porosity: porosity from high-resolution combinable magnetic resource tool.
NMR permeability K_{SDR}: permeability computed using Schlumberger-Doll-Research (SDR) model.
NMR permeability K_{TIM}: permeability computed using free-fluid (Timur-Coates) model.

Figure 14. NMR permeability K_{SDR} computed using Schlumberger-Doll-Research (SDR) and K_{TIM} using Timur-Coates model from two wells 131/08-008-08W2, and 111/01-17-008-06W2, as shown in Figures 13(b) and (c) respectively. Good quantitative relationships are obtained between K_{SDR}, K_{TIM} and TCMR at semi-logarithm axis for Unit A of the Middle Member of the Bakken Formation in the Viewfield Pool.

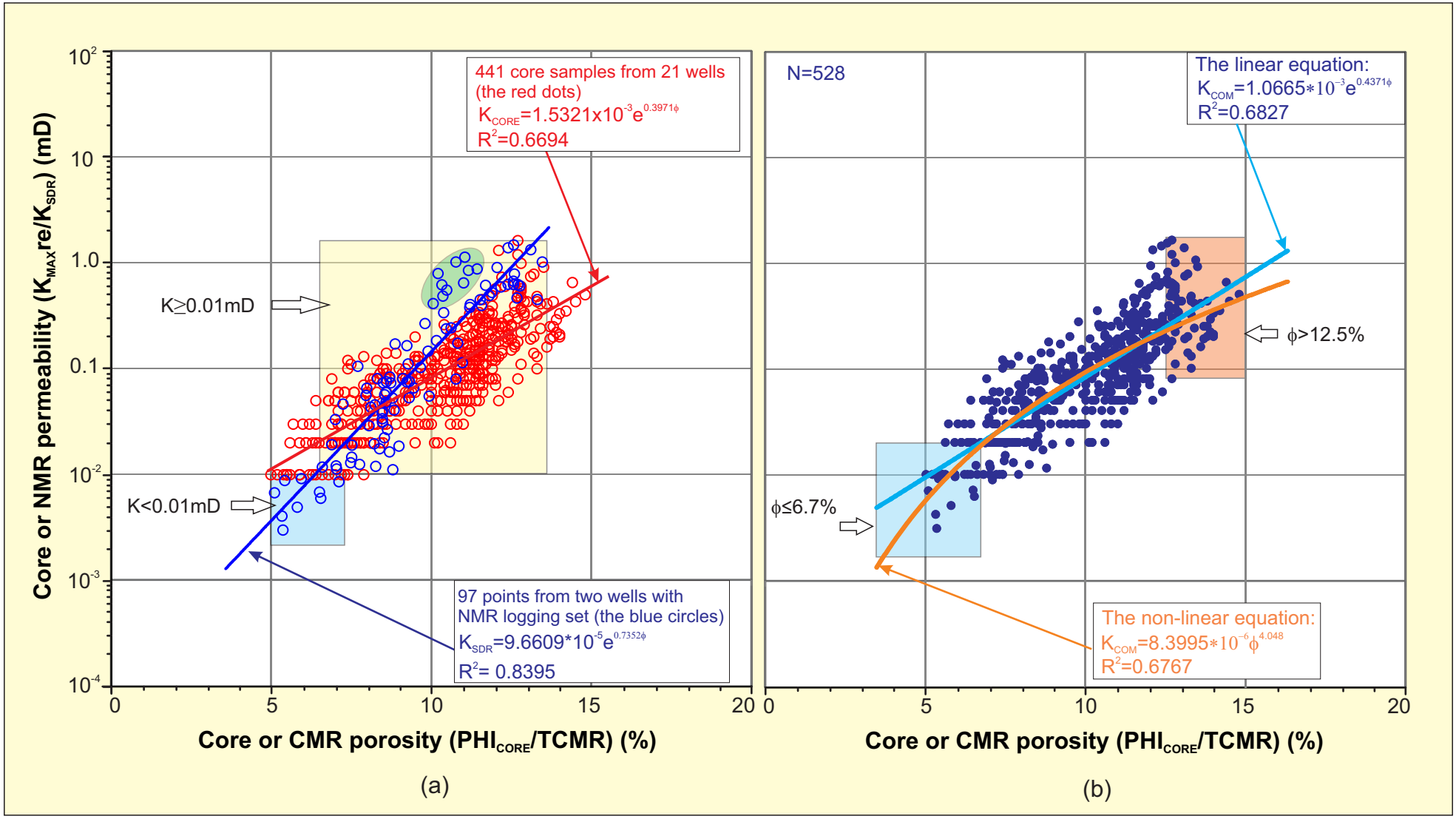

N: number of data points, from 21 cored wells and two wells with NMR data.

Figure 15. Comparison of permeability models for Unit A of the Middle Bakken Member in the Viewfield Pool. (a) - Two relationships, K_{CORE} equation (19), and K_{SDR} equation (20), between permeability and porosity from core analysis and advanced NMR log interpretation. (b) - Relationships between permeability and porosity from combined dataset from core analysis from 21 wells and most of K_{SDR}-TCMR data pairs from two wells, including linear equation (22) and non-linear equation (23) at semi-log axis.

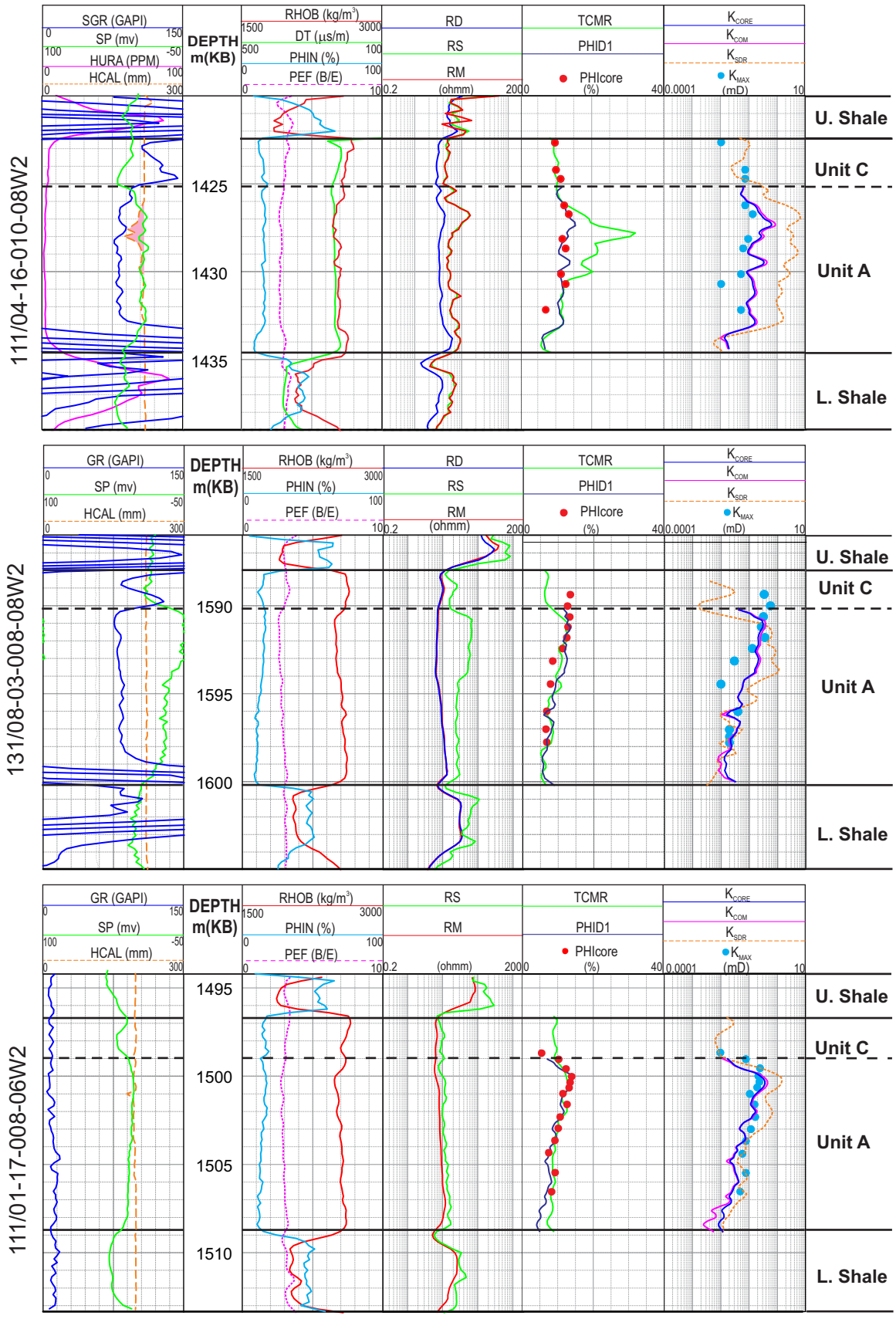

GR - gamma ray log
SGR- spectral gamma ray log
SP - spontaneous potential log
HURA- uranium concentration
HCAL- caliper

RHOB-density log
DT- sonic transit time log
PHIN- neutron porosity log
PEF- photoelectric factor

RD- deep resistivity log
RM- medium resistivity log
RS- shallow resistivity log

TCMR- CMR porosity log
PHID1- calculated density porosity using volume model, equation (7)
PHI_{CORE}- measured core porosity
K_{MAX}- measured core maximum permeability

K_{CORE}- calculated permeability using core-based model, equation (19)
K_{COM}- calculated permeability using combined core-NMR model, equations (22) & (23)
K_{SDR}- NMR permeability log

Figure 16. Examples showing a comparison of NMR porosity and permeability with calculated porosity and permeability derived from proposed porosity and permeability models in this study for Unit A of the Middle Bakken Member for three wells 111/04-16-010-08W2 (a), 131/08-03-008-08W2 (b), and 111/01-17-008-06W2 (c) in the Viewfield Pool of southeastern Saskatchewan.

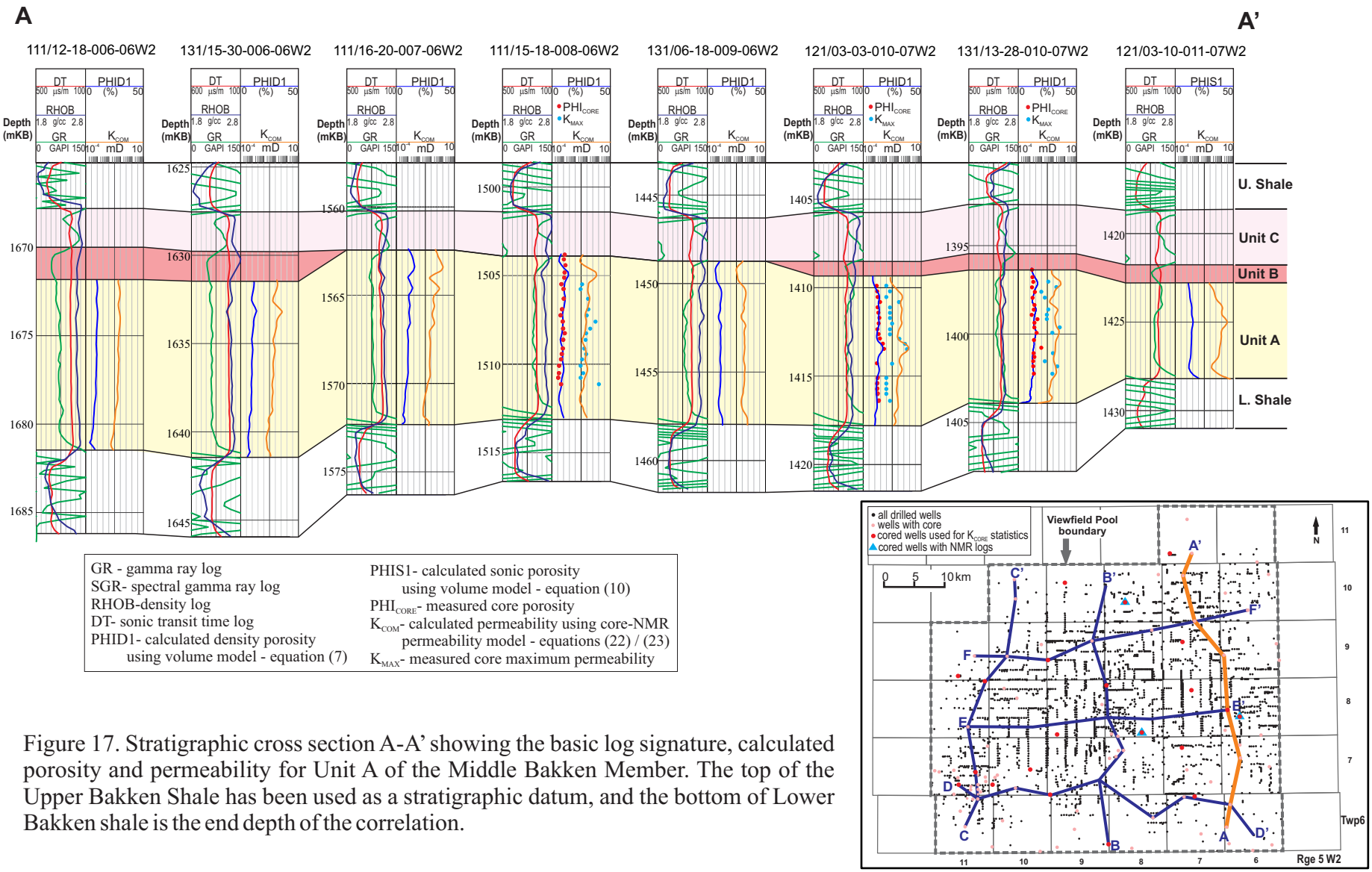

Figure 17. Stratigraphic cross section A-A' showing the basic log signature, calculated porosity and permeability for Unit A of the Middle Bakken Member. The top of the Upper Bakken Shale has been used as a stratigraphic datum, and the bottom of Lower Bakken shale is the end depth of the correlation.

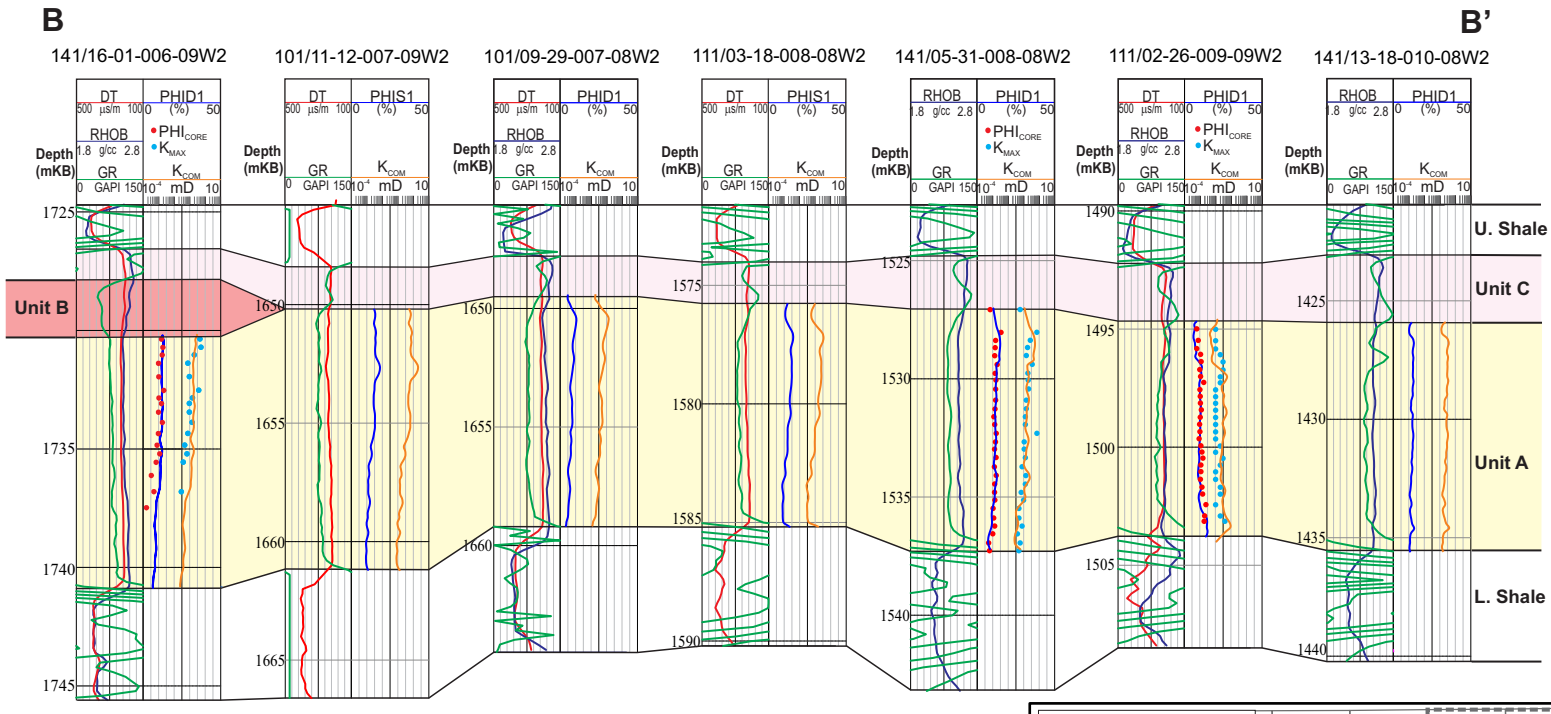

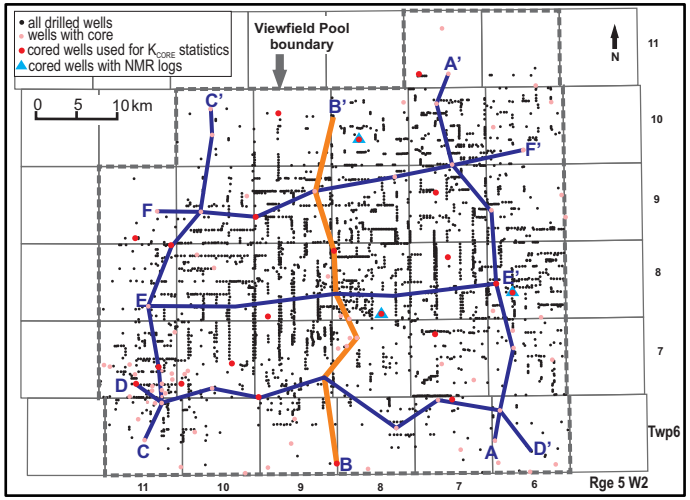

Figure 18. Stratigraphic cross section B-B' showing the basic log signature, calculated porosity and permeability for Unit A of the Middle Bakken Member. The top of the Upper Bakken Shale has been used as a stratigraphic datum, and the bottom of Lower Bakken shale is the end depth of the correlation.

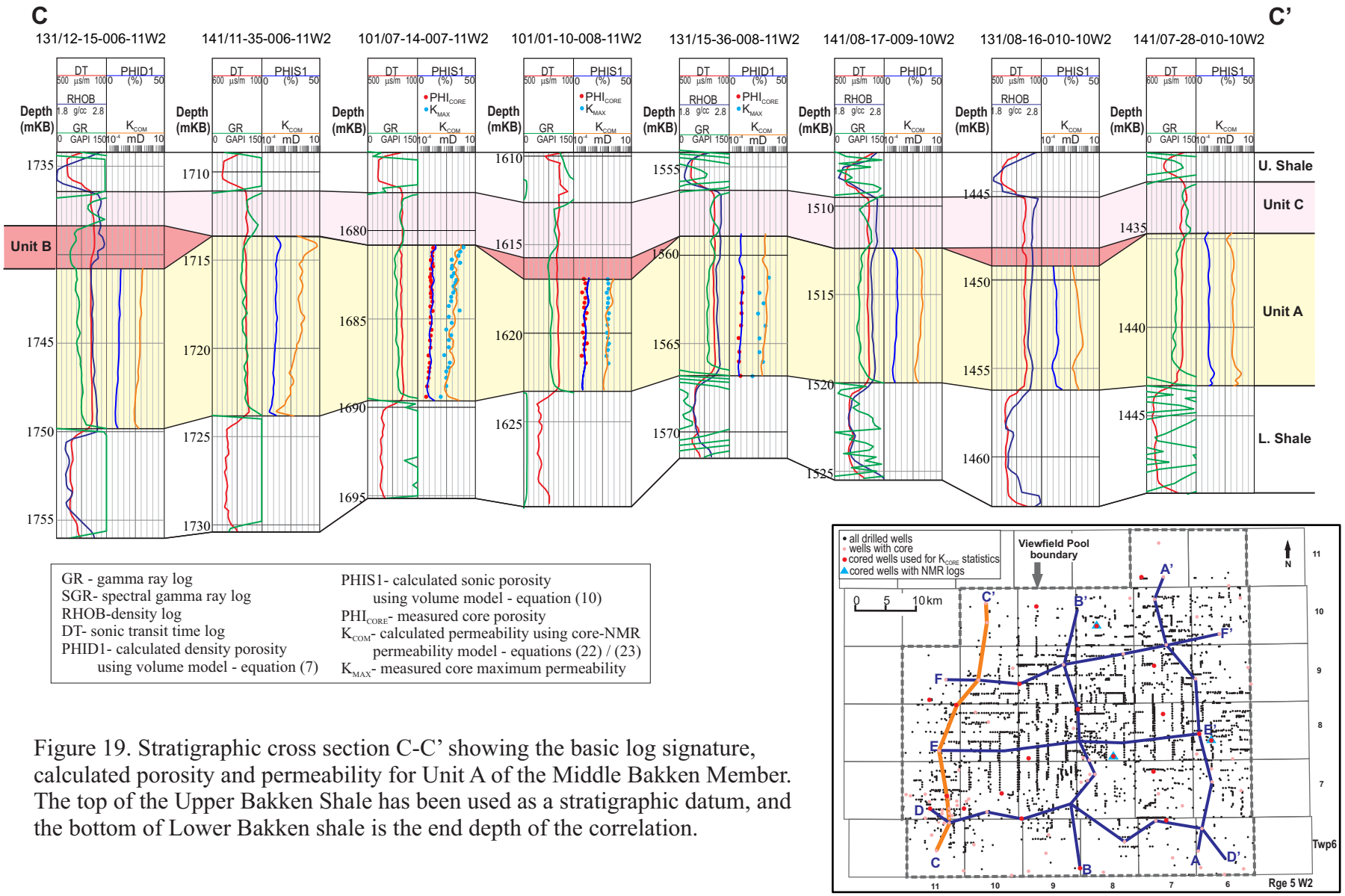

Figure 19. Stratigraphic cross section C-C' showing the basic log signature, calculated porosity and permeability for Unit A of the Middle Bakken Member. The top of the Upper Bakken Shale has been used as a stratigraphic datum, and the bottom of Lower Bakken shale is the end depth of the correlation.

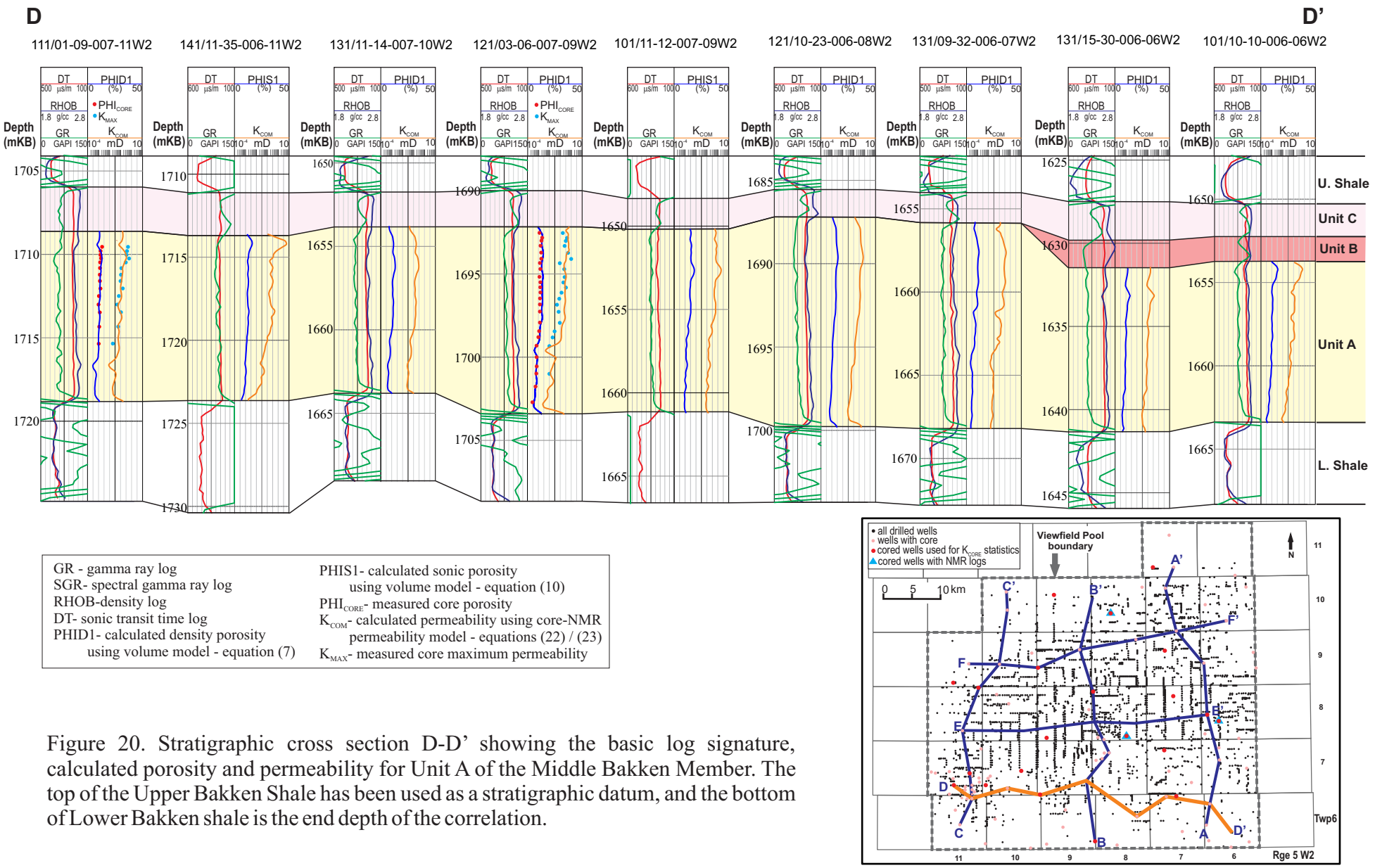

Figure 20. Stratigraphic cross section D-D' showing the basic log signature, calculated porosity and permeability for Unit A of the Middle Bakken Member. The top of the Upper Bakken Shale has been used as a stratigraphic datum, and the bottom of Lower Bakken shale is the end depth of the correlation.

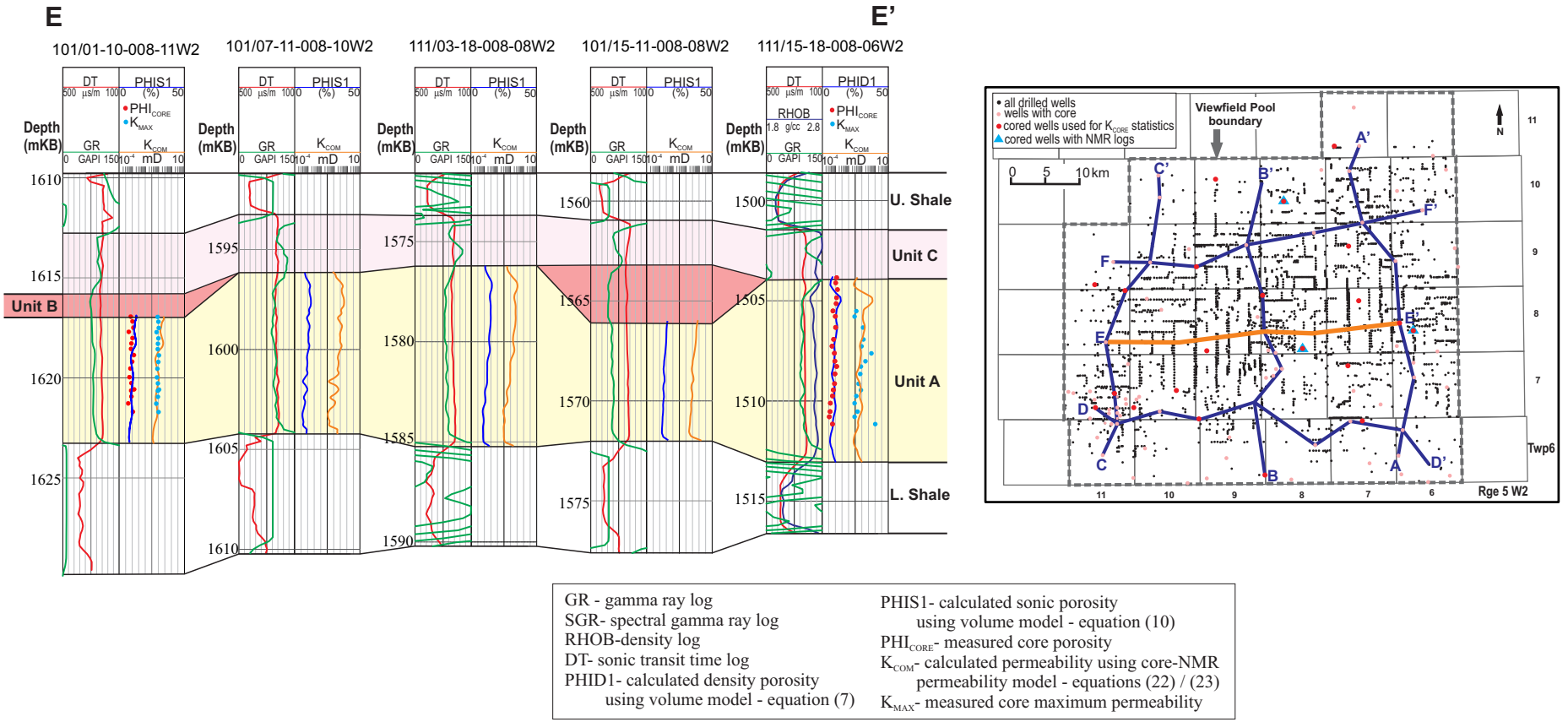

Figure 21. Stratigraphic cross section E-E' showing the basic log signature, calculated porosity and permeability for Unit A of the Middle Bakken Member. The top of the Upper Bakken Shale has been used as a stratigraphic datum, and the bottom of Lower Bakken shale is the end depth of the correlation.

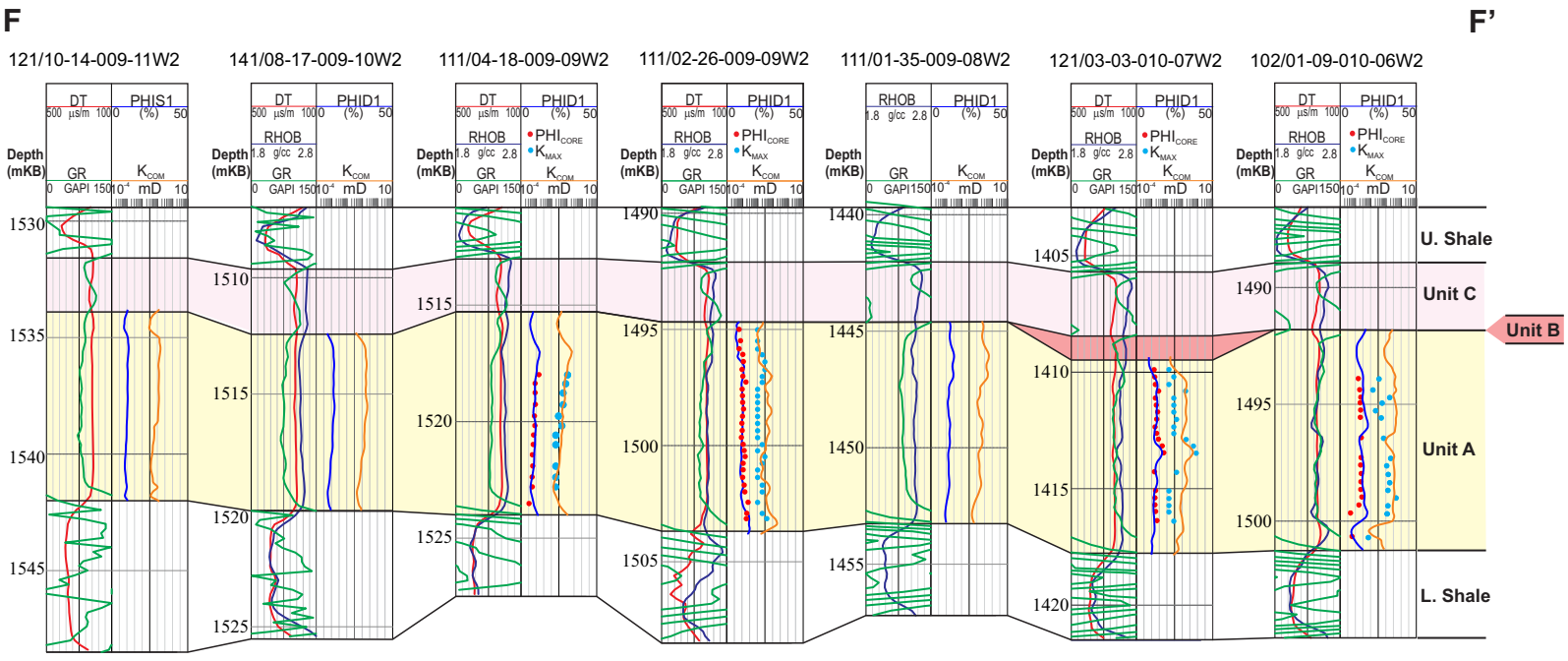

GR - gamma ray log
SGR- spectral gamma ray log
RHOB-density log
DT- sonic transit time log
PHID1- calculated density porosity using volume model - equation (7)
PHIS1- calculated sonic porosity using volume model - equation (10)
PHI_{CORE}- measured core porosity
K_{COM}- calculated permeability using core-NMR permeability model - equations (22) / (23)
K_{MAX}- measured core maximum permeability

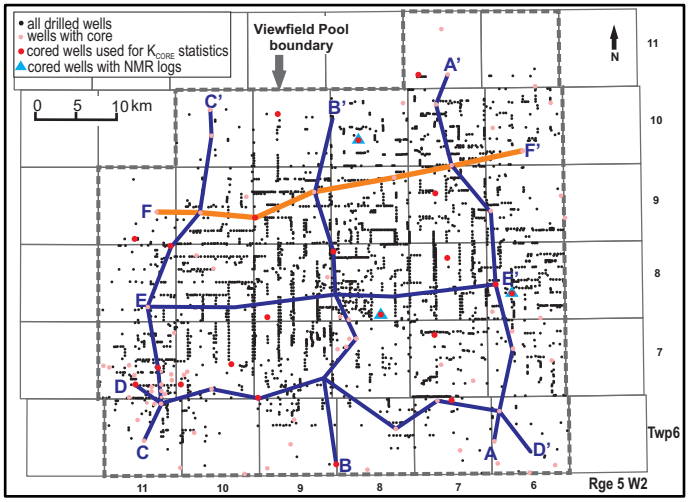

Figure 22. Stratigraphic cross section F-F' showing the basic log signature, calculated porosity and permeability for Unit A of the Middle Bakken Member. The top of the Upper Bakken Shale has been used as a stratigraphic datum, and the bottom of Lower Bakken shale is the end depth of the correlation.